The influence of plate thickness on the fatigue life of transverse k-welds

Eindhoven
University of Technology
the Netherlands

Department of
Mechanical Engineering

The influence of plate thickness on the fatigue life of transverse k-welds

By:
J. Overbeeke
H. Wildschut
F. Paridaans

Report ~~WH~~ 83 - 124

The influence of plate thickness on the fatigue life of transverse K-welds.

by

J.L.Overbeeke *), H.Wildschut **) and F.Paridaans *).

Contents

*) Eindhoven University of Technology, Eindhoven, Holland

**) Metal Institute - TNO, Apeldoorn, Holland

List of symbols

a	crack depth
2b	crack length along the surface
E	Youngs modulus
K_I	S.I.F. = stress intensity factor, mode I
K_f	fatigue notch factor
K_t	s.c.f. = elastic stress concentration factor
n	number of load cycles
N	endurance = number of cycles to failure
R	stressratio, S_{min}/S_{max}
R_m	tensile strength
$R_{p\ 0.2}$	yield strength
S	nominal stress
ΔS	nominal stress range, $S_{max} - S_{min}$
T	plate thickness
σ	local stress
ρ	notch root radius

1. Introduction

Results of research [1, 2, 3] carried out within the ECSC-sponsored first program on the behaviour of steel in marine structures, have shown a distinct influence of the thickness of the plate on the endurance under fatigue loading of welded connections.
However other results [4] within the same program did not show this influence. Therefore, it was decided to gather, within the dutch part of the second research program on steel in marine structures, which was also sponsored by the ECSC, more experimental evidence on this influence of plate thickness on the fatigue life.

The laboratories involved in this sub-program on scale effect were the Laboratories of the Metal Institute - TNO and the
Laboratory for Structural Fatigue, Dept. of M.E., THE.

Fatigue tests at R = 0.1 were carried out on welded, T-shaped joints, having plate thicknesses of 16, 25, 40 and 70 mm respectively.
All specimens were stress-relieved in order to exclude the influence of residual stresses.
The results of these tests are reported here, together with a discussion of the results.

2. Specimens

2.1. Material

The steelplate used for fabrication of the specimens was supplied by Hoogovens BV, IJmuiden, Holland.

- The steel, a normalized carbon-manganese steel, satisfied Euronorm 113-72 requirements for FeE 355 KT.
  The plate was delivered in 4 thicknesses, viz. 16, 25, 40 and 70 mm. The 16 and 25 thick plates were rolled from the same heat. The chemical composition of this heat is given in table 1A. The 40 and 70 mm thick plates were rolled from one other heat. The composition of this latter heat is given in tabe 1B. The mechanical properties of the plates are listed in table 2.

2.2. Dimensions

The specimens were T shaped, see fig. 1, and consisted of strips, 220 mm wide and 800 to 1600 mm long, to which a gusset plate was welded with a full penetration K-weld. The (macro) flange angle of all welds was 60^{o} and the height of the gusset plate was larger than 2.25 times the plate thickness.

- So all testsection profiles were geometrically similar.
- The length of the strips (800 to 1600 mm) was choosen as to agree with the test equipment.

2.3. Welding procedure and post-weld heat treatment

The welding procedure was as follows:
Root welding was done by Manual Metal Arc (MMA) welding.
Subsequently, submerged arc (S.A.) welding was applied for the filling passes. The reason for using SA-welding was a pure economical one.
Finally MMA-welding was applied again for the finishing passes.
The consumables used for MMA-welding were basic-coated, low hydrogen electrodes, confirming to AWS class E7016.

- Full details of the welding procedures used are given in [5].

After welding, all specimens were stress relieved by heating up to 580 ± 20 °C at a mean rate of 200 °C/hour, and after a holding time of 2½ hours, cooling down in the furnace to below 300 °C at a rate of 100 °C/hour. Cooling down from 300 °C to room temperature took place in still air.

Welding and PWHT of the 70 and 40 mm thick specimens was carried out in one batch.
Welding and PWHT of the 25 and 16 mm thick specimens was in 2 batches, designated as I and II resp. in table 3. All specimens contained some form of undercuts and some specimens of batch I were rejected because of undercuts deeper than 0.5 mm as referred to the plate surface. (It should be noted that the limitation of the undercuts to 0.5 mm is arbitrary.) The specimens replacing the rejected ones bear the designation II.
Furthermore, one 16 mm specimen from a small batch (III) used for the evaluation of the welding procedure was tested.

3. Experimental details

3.1. Test conditions

All tests were carried through on servo-hydraulic test equipment.
The 70 mm specimens were tested at the Metal Institute using a machine of 500 kN capacity.
The 40, 25 and 16 mm specimens were tested at Eindhoven University using a machine of 120 kN capacity.
Fig. 2 and 3 resp. show the test set-up.

The specimens were loaded in (almost) pure bending at $R = S_{min}/S_{max} = 0.1$.
The environment was laboratory air with a relative humidity of 40 to 70%.

For each plate thickness, 10 to 11 specimens were available.
As the scale effect to be investigated was expected to be of the same order of magnitude as the spread in endurances, it was decided to test 4 to 5 specimens at one high stress level and 6 to 7 specimens on one low stress level.
The stress ranges were such as to give, according to [4], endurances of approximately $\bar{N} \approx 2 \times 10^5$ ($\Delta S = 200$ N/mm^2) and $\bar{N} \approx 10^6$ ($\Delta S = 120$ N/mm^2) respectively for the specimens with 40 mm plate thickness.

3.2. Stress control

As the 70 mm specimens were loaded in 4-point bending, see fig. 2, load control provided sufficient accuracy for stress controlling the specimens. However, this was not the case for the other specimens. As these were loaded in bending by highly excentric normal forces, see fig. 4, the angular misalignment, due to welding on one side of the plate only, influenced the bending moment.
As this misalignment amounted to an increase of excentricity up to 15 mm for the 16 mm specimens, where total excentricity was ∿200 mm, all specimens were monitored by straingages (½ wheatstone bridge for bending, assumed modulus: E = 210,000 N/mm^2).

These straingages were situated, see fig. 4, at the longitudinal centre-line of the specimen at a distance ∿130 mm (40 mm spec.) to ∿120 mm (16 mm spec.) from the weld toe.
As these distances are >> t from the weld toe, these gages were not in influenced by the stress concentration of the weld.
The accuracy of the load monitoring, taking into account the effects of the normal stresses and of the biaxial strainfield, was 0 to -3%.
On the other hand, the stresses in the 70 mm specimens followed directly from the applied load (4-point bending).

3.3. Crack growth monitoring

During all tests, except those of series A70, visual inspection with a magnifying glass was carried out more or less regularly (that is: within working hours).
Plots of the observed cracklengths, 2b, against the number of cycles are given in fig. 5 through 7.
In these figures, the observed cracklengths are given as arrows. These arrows are interconnected by continuous curves for that side of the gusset plate where the failure finally took place, and by dashed curves for the other side.

The smallest cracks observed were appr. 4 mm. They often started from small but rather sharp undercuts.
Because haircracks of this size are difficult to detect on the one hand and often seem to be non-propagating for a very long time (see e.g. spec. A25-9) on the other, the number of cycles at "initiation" as given in table 3, coincides with a crack length of ∿10 mm at that side of the gusset plate were failure took place.

- A specimen was regarded as "failed" when the crack was half-way through the thickness at the sides of the specimens. When the crack had progressed to that level, the remaining unbroken area was, due to the curved crackfront, less than 40% of the original area.
  The cracklength at the non-failed side of the gusset plate at the endurance N is also given in table 3. From this table it seems that there is either a large crack or no crack at all.

4. Results and analysis

4.1. ΔS-N curves

The test results of all specimens are given in table 3, and the endurances are plotted per series in fig. 8 through 11.
As it was shown in [4] that a Basquin-type equation, $\Delta S^m N = C$, is applicable to this type of specimen, it was applied here too.
The results, determined by linear regression, are as follows:

- Series A70 - 60 - 1 - XNLG

$$3.527 \log \Delta S + \log N = 13.315 \qquad (1)$$

- Series A40 - 60 - 1 - XNLG

$$4.159 \log \Delta S + \log N = 14.798 \qquad (2)$$

- Series A25 - 60 - 1 - XNLG

$$4.066 \log \Delta S + \log N = 14.680 \qquad (3)$$

- Series A16 - 60 - 1 - XNLG

$$4.244 \log \Delta S + \log N = 15.215 \qquad (4)$$

It should be noted that the specimens A70 - 60 - 1 - 3NLG and A16 - 60 - 1 - 11NLG, both at $\Delta S = 120$ N/mm^2, are not taken into account for calculating eq. (1) and (4).
The A70 specimen is a run-out at $N > 5.7 \times 10^6$, and the A16 specimen is almost a run-out as $N = 8.3 \times 10^6$.
Therefore these two specimens are regarded as belonging to the scatterband of the fatigue limit, and not to the scatterband of the ΔS-N curve.

Equation (1) through (4) are plotted in the appropriate figures. All results, together with the regressionlines are plotted in fig. 12.
Fig. 13 shows the regressionlines together with the regressionline for all specimens together viz.:

- Series A70 through A16

$$4.026 \log \Delta S + \log N = 14.559 \qquad (5)$$

4.2. Effect of plate thickness

Fig. 12 shows that the scatterband of all series together comprises only a factor 3 at the higher stress range and a factor 5 at the lower one. The influence of the plate thickness, however, is small but clear.
To evaluate this influence, the mean values and the standard deviations of log N were calculated per series and per stressrange. These results are given in table 4, and plotted per stressrange on the base of $\overline{\log N}$ versus log T in fig. 14.
The lines in this figure, which are drawn to the eye, correspond to

$$1.6 \log N + \log T = f(\Delta S). \qquad (6)$$

for both stressranges. However it is clear that for the high stressrange, eq. (6) is only valid for a thickness up to ∿32 mm. At larger plate thicknesses the effect seems to level off.
A possible reason is given in par. 5.3.

Incorporating eq. (6) into eq. (5) yields:

$$4.0 \log \Delta S + \log N = C - 0.625 \log T \qquad (7)$$

The relation between ΔS and T at a constant value of the endurance N is

$$6.4 \log \Delta S + \log T = \text{constant} \qquad (8)$$

or, using a set of reference values N_o, ΔS_o, T_o:

$$N = N_o: \qquad \frac{\Delta S}{\Delta S_o} = \left(\frac{T_o}{T}\right)^{0.156} \qquad (9)$$

5. Discussion

5.1. Crack initiation and growth

The picture, emanating from fig. 5, 6 and 7 and from visual observation is as follows:
At a few sites, where the geometrical- and/or metallurgical and/or residual stress conditions are favourable, haircracks are initiated at an early stage of life, see fig. 15.
Undercuts and local increased reinforcements seem to be the most favourable sites for crack initiation.
These cracks grow very slowly along the surface, although they may grow quicker into the depth. Very often they seem to become non-propagating although their lengths can be up to 6 mm, see e.g. fig. 6a.

- In a later stage of the life, a larger or large number of secondary initiations seems to occur, probably at less favourable sites. When some of these grow in the neighbourhood of an existing haircrack, they will undergo the influence of its stressfield, grow more quickly and soon line-up with the haircrack. This shows up on the fracture surface as a step. See fig. 15, fig. 16 and fig. 17.
  When these secondary cracks have amalgamated with the larger haircrack, the crackfront in depth direction is no more compatible with the stress field, and the crack grows now predominantly in the depth direction.
  When crackfront and stressfield match again, tertiary cracks will have grown along the melting line under the influence of the stressfield of the main crack. These will line up again with the main crack and the above sketched process will repeat itself until the main crack or cracks reach the edges of the specimen.

5.2. Geometrical scale effect

The influence of specimen dimensions on the endurance of notched specimen has 3 roots.

5.2.1. The stress concentration factor (s.c.f.)

When all dimensions are scaled up except the notch root radius ρ, as in the case of welded joints, the s.c.f., K_t, increases because of a decreasing ratio ρ/T (T = thickness of the plate), that means a relatively sharper notch, see fig. 18.

5.2.2. The stress gradient near the notch root.

The relative gradient of the maximum principal stress, $\frac{d\sigma/dx}{\sigma_{max}}$, see fig. 19, is dominated by the notch root radius [7] and the same, see fig. 20, holds for the S.I.F. of small cracks emanating from this root [8].

It follows that, for welded joints, crack initiation and the growth of small cracks are a function of the details of the weldtoe profile and the s.c.f. only.

When the weldtoe profile is regarded as independent of specimen size, the scale effect in the regime of small cracks is dominated by K_t, the s.c.f.

5.2.3. The stress gradient outside the notch root region.

When specimen dimensions increase, the stresses outside the region dominated by ρ, as discussed in par. 5.2.2., level off more slowly (when the nominal stress is supposed to be the same,), see fig. 21.

It follows that the S.I.F. for a certain crack depth is higher for the larger specimen.

As integration of Paris law, together with observations of crack length against number of cycles, as e.g. shown in fig. 5, 6 and 7, show that the major part of the endurance is determined by the growth of the smaller cracks, a scale effect results.

5.3 Influence of stress range.

Fig. 14 shows that the influence of the plate thickness at $\Delta S = 200$ N/mm^2 reduces sharply for T > ∿32 mm, and in the following it is shown that this is most probably due to plasticity effects.

From [9] Ch. 3, it follows that the fatigue strength at R = 0 and N = $2,10^6$ for machined, unnotched specimens is: $\Delta S_{R=0} \approx 0.77\ R_m$.
With $R_m \approx 540$ N/mm^2, see table 2, it follows that $\Delta S_{R=0} \approx 400$ N/mm^2, and slightly higher than $R_{p\ 0.2}$.

From fig. 13 it follows that at N = $2,10^6$ holds $\Delta S_{R=0,1} \approx 110$ N/mm^2, resulting in $K_f \approx 400/110 \approx 3.6$, which will correspond to $K_t \approx 4$.
Now it follows that at $\Delta S = 200$ N/mm^2 and R = 0,1 the calculated maximum elastic stress range is about equal to the Yieldstress range.

$\sigma_{max,\ elast.} \approx K_t.\Delta S = 4 \times 200 = 800$ N/mm^2 $\approx 2\ R_{p\ 0.2}$.

It follows that:

- the loading at the notch root is of the low-cycle fatigue type
- the initial plastic zone size is of the order of the notch root radius, at least for the thicker material.

And this will result in a smaller scale effect for specimens with a large plastic zone size due to a flat stress gradient, see par. 5.2.
Why the change-over is, see fig. 14, rather abrupt, is not clear, but the relatively low yield strength of the 70 mm material could be of influence.

5.4. Comparison with other results

Models for calculating the scale effect described in par. 5.2. use a root radius $\rho = 0$ and an initial crack length a_i of a fixed length, corresponding to an average size weld defect.
Fig. 22 shows results reported in [10] together with the results from this investigation, and it appears that the experimental scale effect is larger, most probably due to the effects described in par. 5.2.1. and 5.2.2.

A more elaborate model, used in [1], incorporates the weld toe radius, the weld toe angle and also accounts for crack-ellipticity for cracks up to 3 mm deep.
Analytical results based on the actual geometry of the welded specimens are given together with the experimental ones and a very good correlation is shown.
Fig. 23 shows the experimental results from [1] together with the results from table 4 and it appears that the scale effect from [1] is higher than reported here.
However, the differences in specimen geometry and in loading condition, together with the differences in weld geometry (root radius and toe angle) per plate-thickness, make a direct comparison not well possible.

Comparison with results from [2,3] is not possible, because in said investigations the technological aspects were paramount.

6. Conclusions

From an investigation into the effect of plate-thickness on the endurance of T shaped, welded specimens for which the geometry and welding parameters at the toe of the weld were essentially kept the same, it follows that:

1. The endurance decreases with the thickness to the power 5/8 for low stressrange levels.

$$\Delta S = 120\ N/mm^2 : \left(\frac{N_1}{N_2}\right) = \left(\frac{T_2}{T_1}\right)^{0,625}$$

2. This results, with an ΔS-N curve as measured of the form $\Delta S^4 . N = C$ in

$$N = 2,10^6 ; \qquad \frac{\Delta S_1}{\Delta S_2} = \left(\frac{T_2}{T_1}\right)^{0.156}$$

3. At high stress levels ($\Delta S = 200\ N/mm^2$), the thickness effect reduces to almost zero for $T > 32$ mm. Most probably this is due to effects of cyclic plasticity.

4. Analytical results show that the scale effect can be split up into 2 parts, viz:
   - A scale effect due to the radius ρ at the weld toe, which is dominated by $K_t = f(\rho/T)$ and which influences crack initiation and the growth of small cracks.
   - A scale effect for small to medium size cracks because of the stress gradient across the specimen.

Acknowledgement

This research was performed with financial aid of the European Committee under contract number CECA 7210-KG/601.

References

1. S. Berge and K. Engesvik: Effect of the plate thickness in fatigue of transverse fillet welds. Int. Conf. on Steel in Marine Structures, paper 2.5., Paris, October 1981.

2. R. Olivier et al. : Untersuchungen zur Korrosionsermüdung von Offshore-Konstruktionen unter einstufige Belastung. ibid. paper 2.4.

3. R. Olivier et al. : Untersuchungen zur Korrosionsermüdung von Offshore-Konstruktionen unter seegangtypischer Belasting. ibid. paper 7.1.

4. J.L. van Leeuwen et al. : Constant amplitude tests on welded steel joints performed in air and seawater. ibid. paper 2.1.

5. J. de Back et al. : Final Report to ECSC-Convention 7210 - KG - 601. To be published, 1984.

6. M.H.J.M. Zwaans et al. : The endurance of a welded joint under two types of random loading. Int. Conf. on Steel in Marine Structures . Paper 7.3., Paris, October 1981.

7. J. Schijve : Stress gradients arount notches. Report LR - 297. Dept. of Aerospace Eng., Delft University of Technology, 1980.

8. J. Schijve : The stress intensity factor for small cracks at notches. Report LR - 330, ibid, 1981.

9. T. Gurney : Fatigue of welded structures.
Cambridge University Press, 1979.

10. T. Gurney : The influence of thickness on the fatigue strength of welded joints.
Boss '79, paper 41, London 1979.

Table 1 Chemical composition of the materials used

A. Chemical composition of the heat from which the 16 and 25 mm plates were rolled.

C	0.18	Cu	0.03	
Mn	1.45	Cr	0.03	
P	0.020	Ni	0.031	$C_{eq} = 0.429$
S	0.014	Mo	0.03	
Si	0.20	Nb	0.026	
Al	0.05			

B. Chemical composition of the heat from which the 40 and 70 mm plates were rolled.

C	0.17	Cu	n.d.	
Mn	1.45	Cr	n.d.	
P	0.015	Ni	n.d.	$C_{eq} < 0.45$
S	0.004	Mo	n.d.	
Si	0.31	Nb	0.038	
Al	0.040			

Table 2 Dimensions and mechanical properties of plates used for fabrication of the specimens.

thickness mm	rolling number (steel plate designation)	dimension of plate length x width x thickness mm	R_e N/mm^2	R_m N/mm^2	Elongation dp5 %	Charpy-V Energy J at (°C)
16	T7372	2100 x 2000 x 16	411	556	29.3	82 (-40)
25	T7371	2100 x 2000 x 25	401	549	26.7	128 (-40)
40	71214	7000 x 2250 x 40	408	550	31.0	143 (-30)
	71215	7000 x 2250 x 40	414	562	32.0	160 (-30)
70	V9160	5000 x 2100 x 70	378	533	30.5	146 (-30)

Table 3a Test results Series A70 and A40

Environment: air, r.h. 40 - 70%
Loading : bending, R = 0.1

Specimen	Batch	Date of test (average)	Freq. Hz	Stress Range N/mm^2	$N \times 10^{-3}$ at 2b = 10 mm	Endurance $N \times 10^{-3}$	2b at the other side mm	remarks
A70 - 60 - 1 - 3 NLG		20-10-82	2	120	not determ.	>5700	none	run-out
9		12-11-82	2	120	n.d.	1338	17	
4		25-11-82	2	,,	n.d.	1040	40	
2		1-1-83	2	,,	n.d.	1010	53	
12		9-12-82	2	,,	n.d.	1006	-	
7		20-4-83	2	,,	n.d.	755	none	
1		14-6-83	2-4	,,	n.d.	718	none	
5		17-11-82	2	-		-		overloaded
6		18-9-82	2	200	n.d.	190	63+30	
3		30-10-82	2	,,	n.d.	158	23+18	retest
11		10-1-83	1	,,	n.d.	152	18	
8		12-6-83	1	,,	n.d.	147	23	
10		10-2-83	2	,,	n.d.	146	none	
A40 - 60 - 1 - 10 NLG		16-8-82	9	120	n.d.	1875	none	
5		21-6-82	8.6	,,	1150	1809	213	
8		2-10-82	9	,,	~ 1000	1388	none	
7		21-6-82	8.6	,,	n.d.	1345	none	
4		16-8-82	9	,,	n.d.	1218	125	
3		26-9-82	5	,,	n.d.	1060	45	
9		7-9-82	6.6	200	n.d.	193	181	
1		7-9-82	6.6	,,	n.d.	189	214	
2		21-9-82	5	,,	n.d.	141	134	
6		21-9-82	5	,,	~ 85	161	154	

Table 3b Test results Series A25 and A16

Environment: air r.h. 40 - 70%
Loading : bending R = 0.1

Specimen	Batch	Date of test (average)	Freq. Hz	Stress Range N/mm^2	N x 10^{-3} at 2b = 10 mm	Endurance N x 10^{-3}	2b at the other side mm	remarks
A25 - 60 - 1 - 1 NLG	I	14-3-83	7	120	∿1100	2323	160	
4	I	25-2-83	7	,,	n.d.	1893	144+12	
9	II	17-2-83	7	,,	1400	1814	200	
3	I	14-3-83	7	,,	n.d.	1702	88	
10	II	17-2-83	7	,,	n.d.	1448	26+4	
12	II	25-2-83	7	,,	n.d.	1164	none	
11	II	-		-		-		not tested
6	I	14-12-82	5	200	∿135	218	203	
5	II	7-3-83	5	,,	115	215	none	
7	II	7-3-83	5	,,	∿115	208	174	
8	I	14-12-82	5	,,	n.d.	204	155	
A16 - 60 - 1 - 11 NLG	III	8-4-83	5	120	n.d.	8443	none	
5	II	8-7-83	5	,,	n.d.	3253	118+35	
6	I	9-5-83	5	,,	∿1200	3242	168	
4	I	2-6-83	5	,,	2350	3058	none	
8	II	8-4-83	5	,,	1300	2466	none	
10	II	9-9-83	5	,,	n.d.	1691	none	
2	II	8-7-83	5	,,	n.d.	1672	none	
7	I	5-7-83	4.4	200	250	360	169	
3	I	5-7-83	4.4	,,	∿1600	319	190	
1	II	23-6-83	4.4	,,	n.d.	238	none	
9	II	23-6-83	4.4	,,	n.d.	232	172	

Table 4 Summary of test results.

stress range	plate thickness	No of spec.	mean life		stand-deviation	
			$\overline{\log N}$	cycles x 10^{-3}	$\sigma(\log N)$	$\sigma(N/\bar{N})$
N/mm^2	mm					
120	70	6 *)	5.981	957	0.100	1.26
	40	6	6.152	1419	0.097	1.25
	25	6	6.227	1685	0.103	1.27
	16	6 *)	6.392	2466	0.136	1.37
	all	24	6.188	1541	0.203	1.60
200	70	5	5.198	158	0.047	1.11
	40	4	5.230	170	0.064	1.16
	25	4	5.325	211	0.013	1.03
	16	4	5.451	282	0.094	1.24
	all	17	5,301	200	0.114	1.30

*) ex specimen A16 - 60 - 1 - 11 NLG

,, ,, A70 - 60 - 1 - 3 NLG

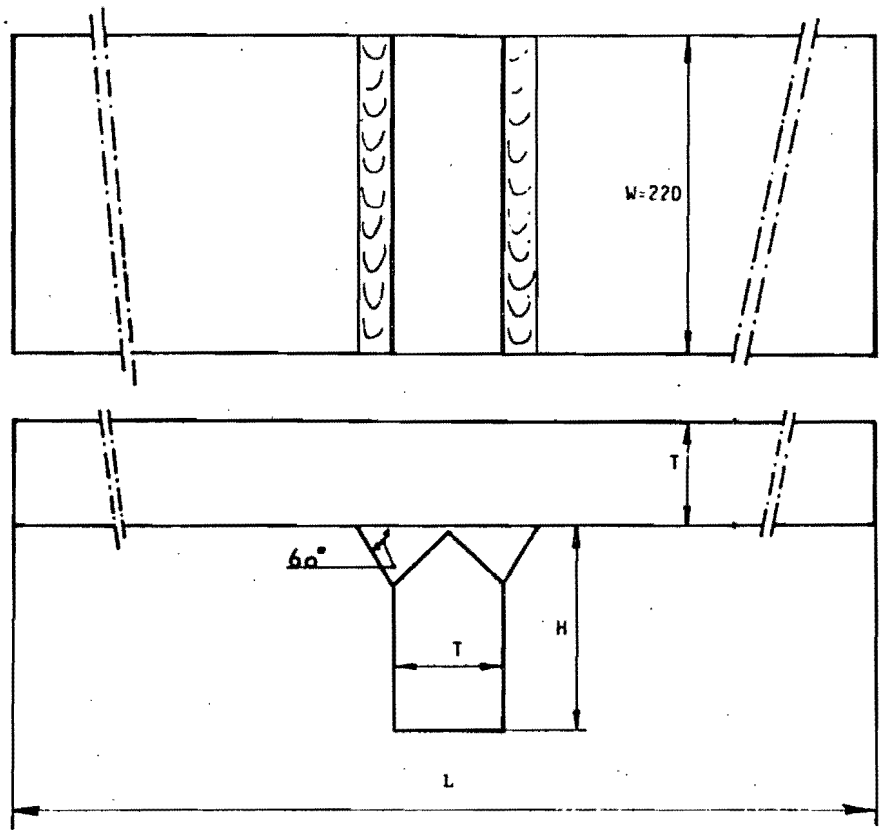

thickness T	length L	height H	width W	(mm)
16	800	37	220	
25	800	57	220	
40	920	90	220	
70	1600	160	220	

fig.1 Geometry and dimensions of test specimens (welded T-joints)

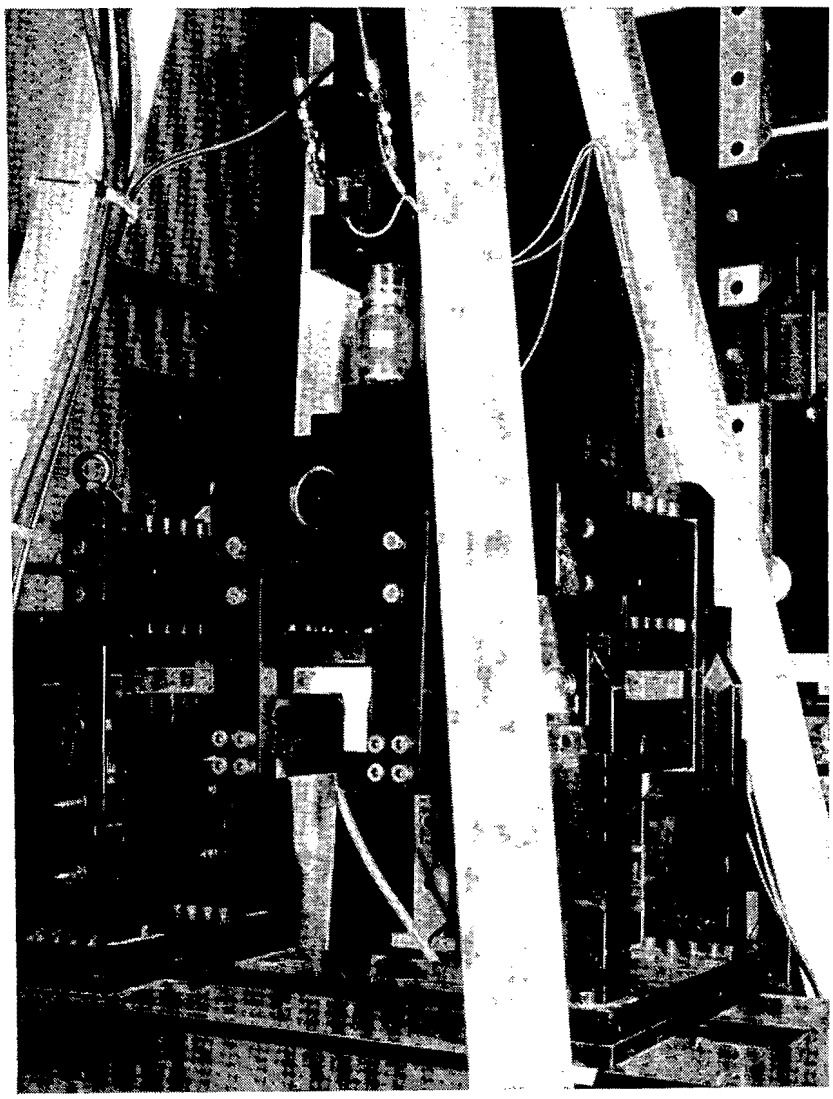

fig. 2. Test set-up at the Metal Institute

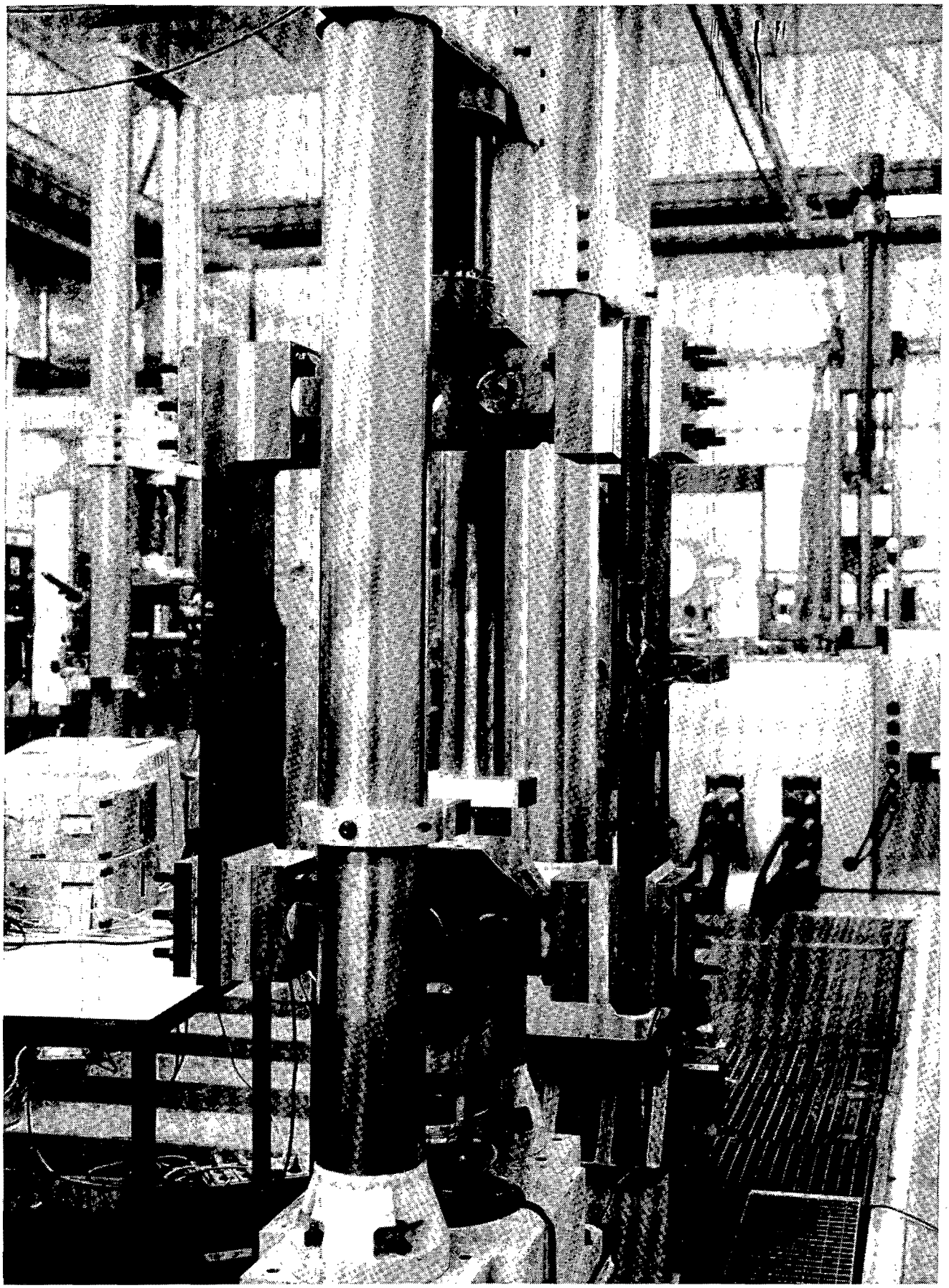

fig. 3. Test set-up at Eindhoven University.

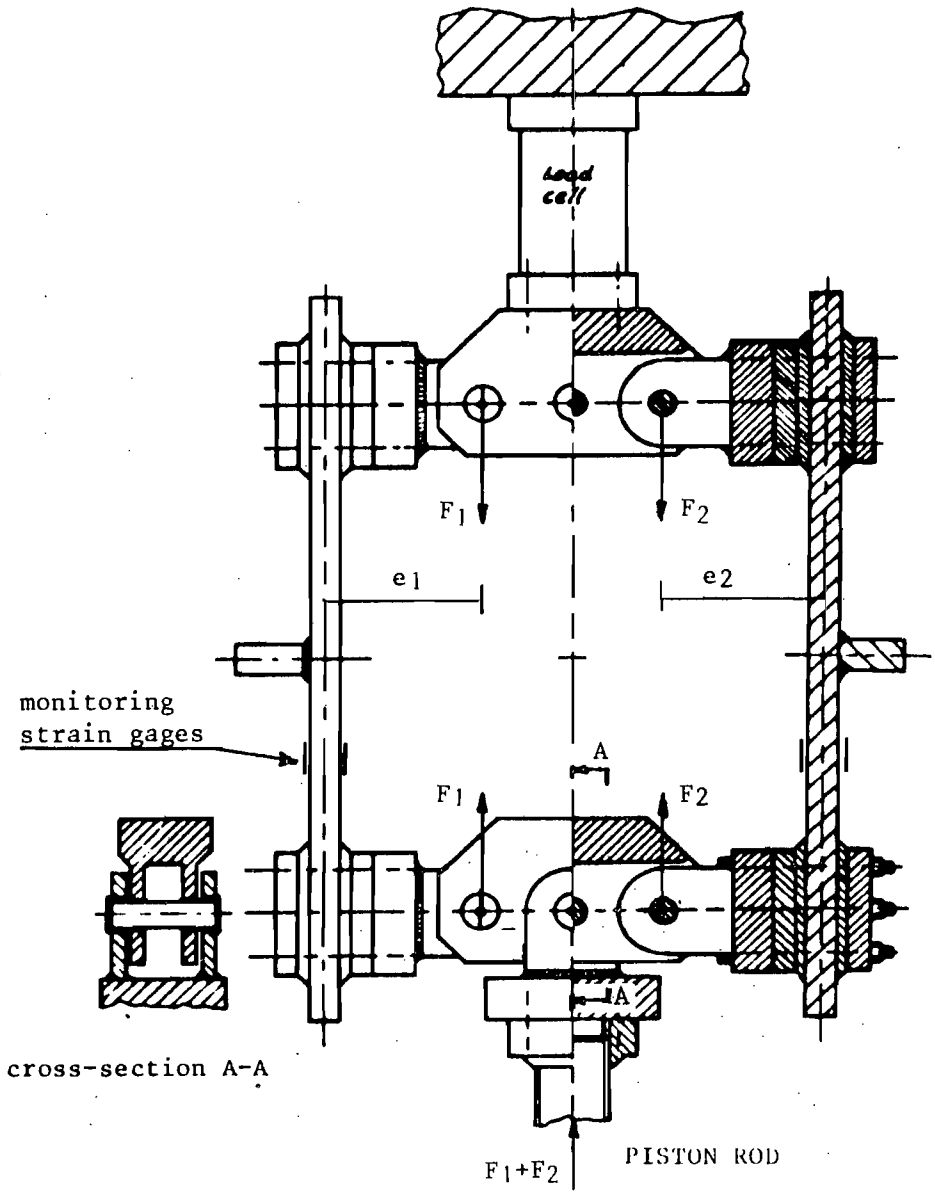

fig. 4 Test setup at Eindhoven University. Schematic

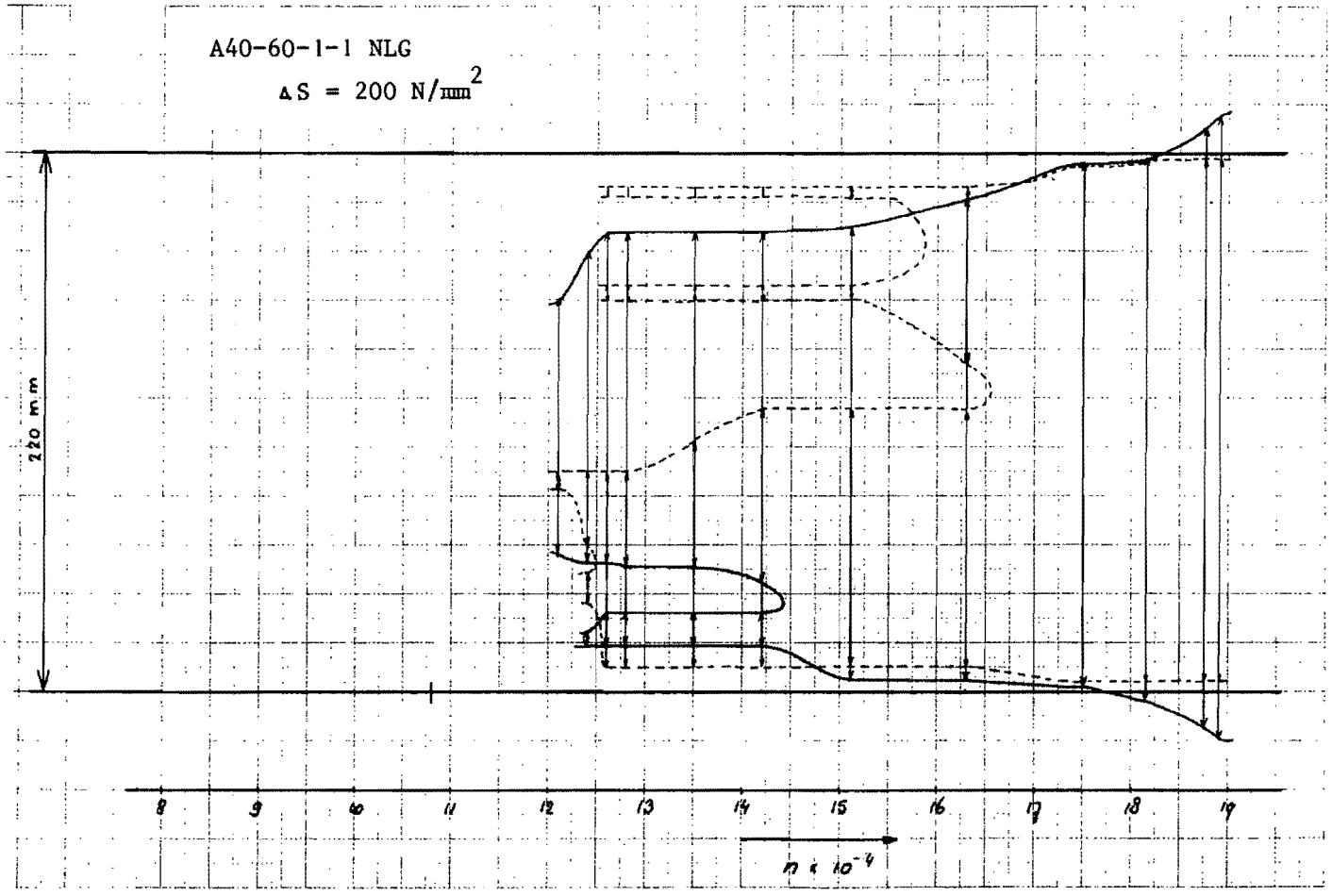

fig. 5a Crack growth measurements, specimens series A40

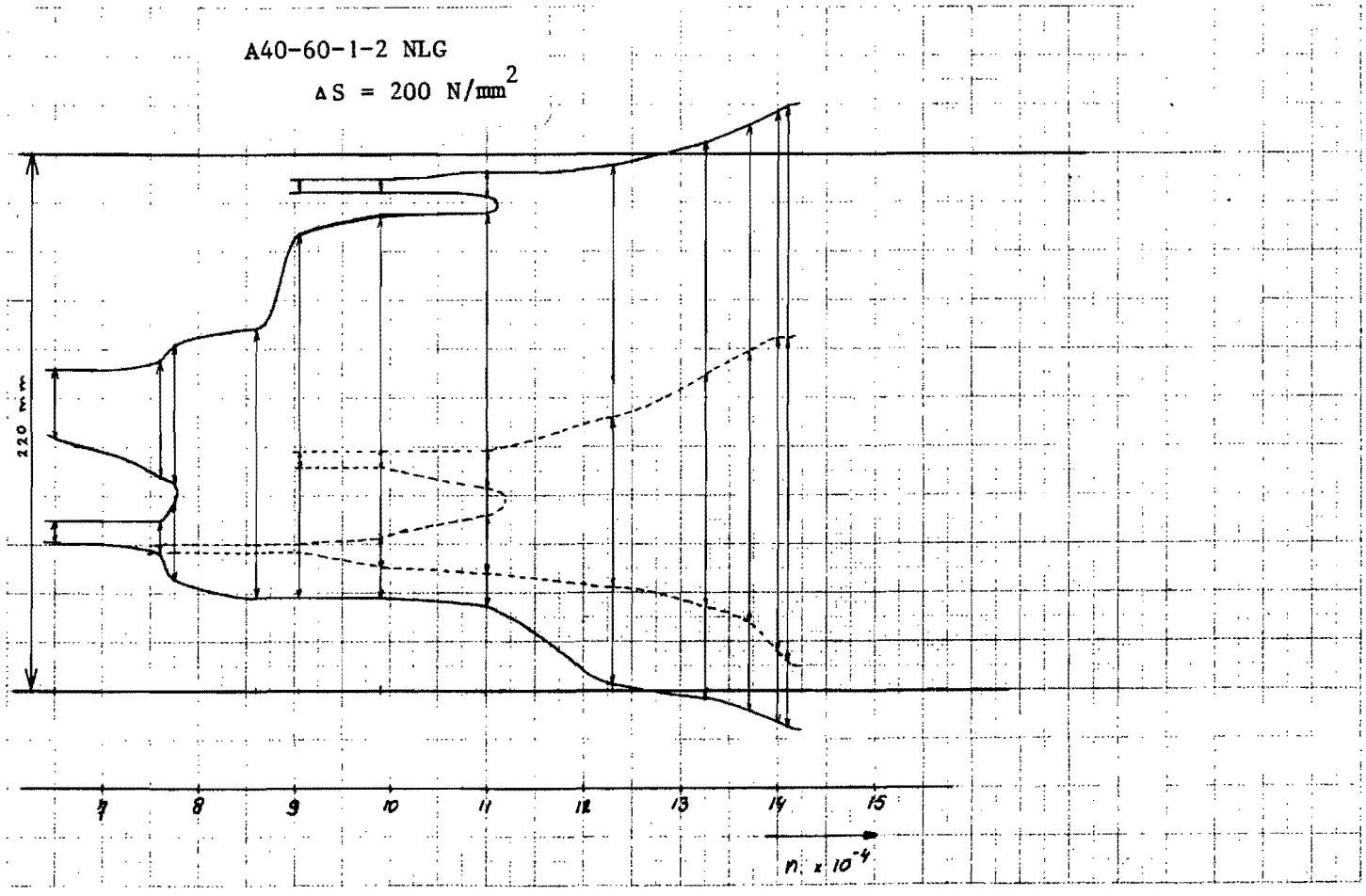

fig. 5b Continued

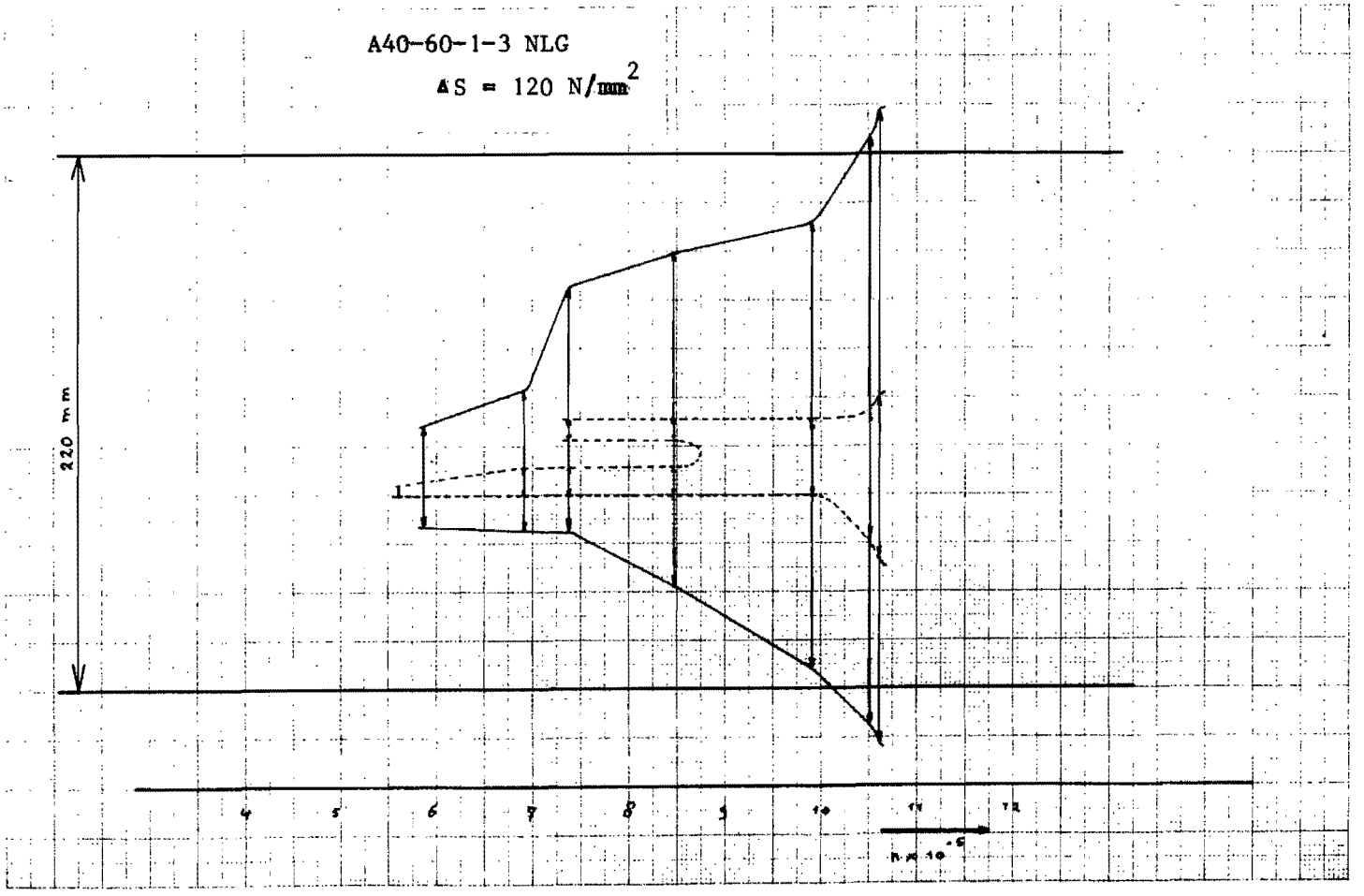

fig. 5c Continued

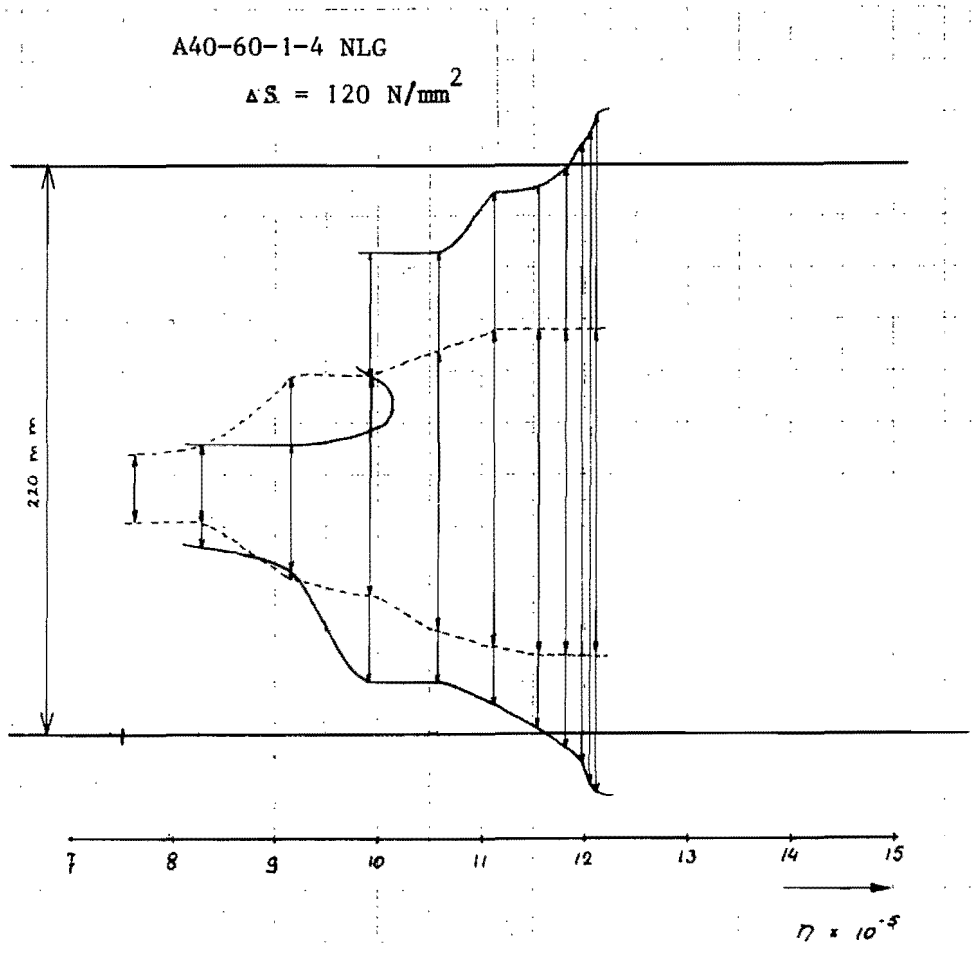

fig. 5d Continued

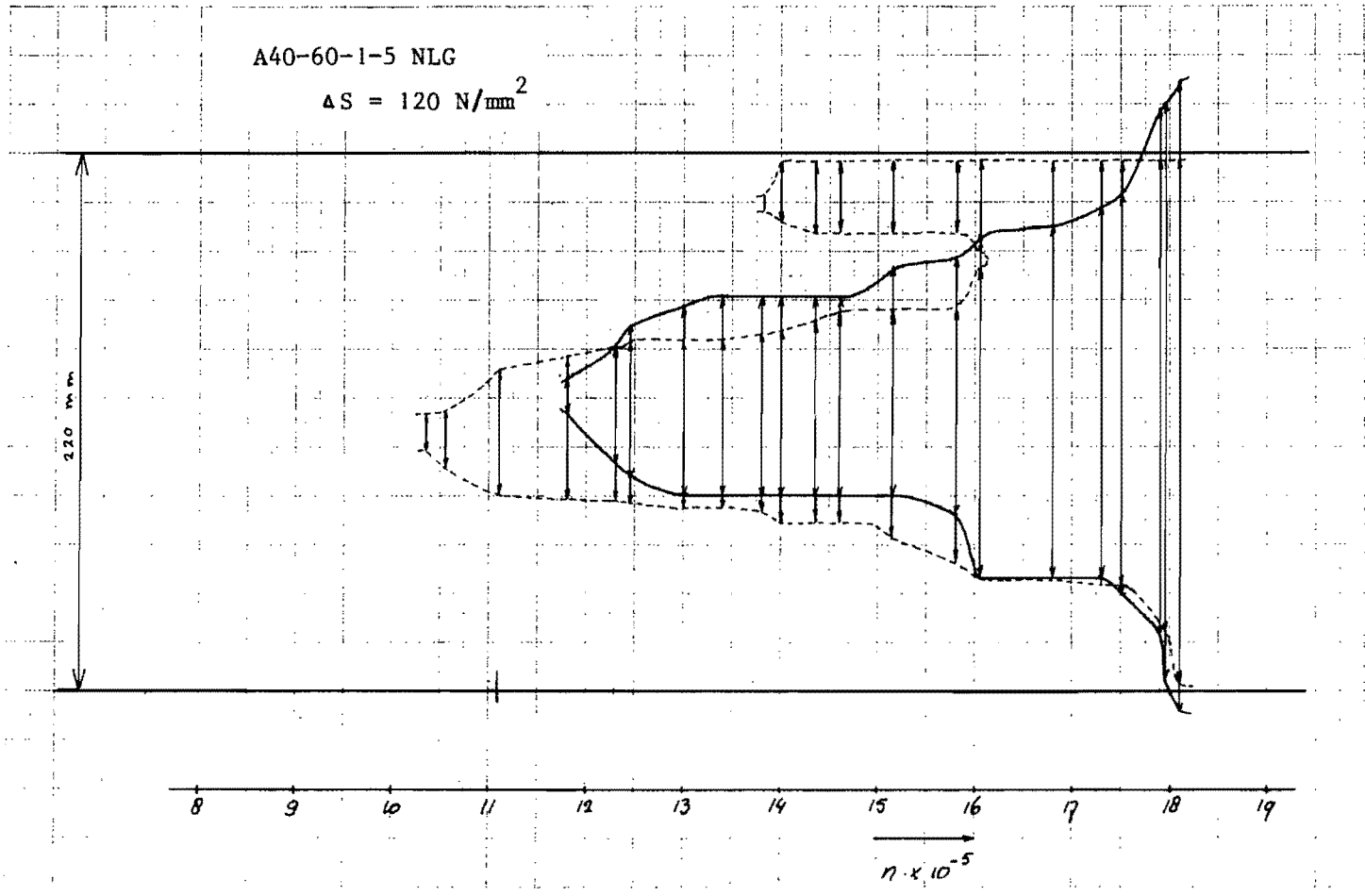

fig.5e Continued

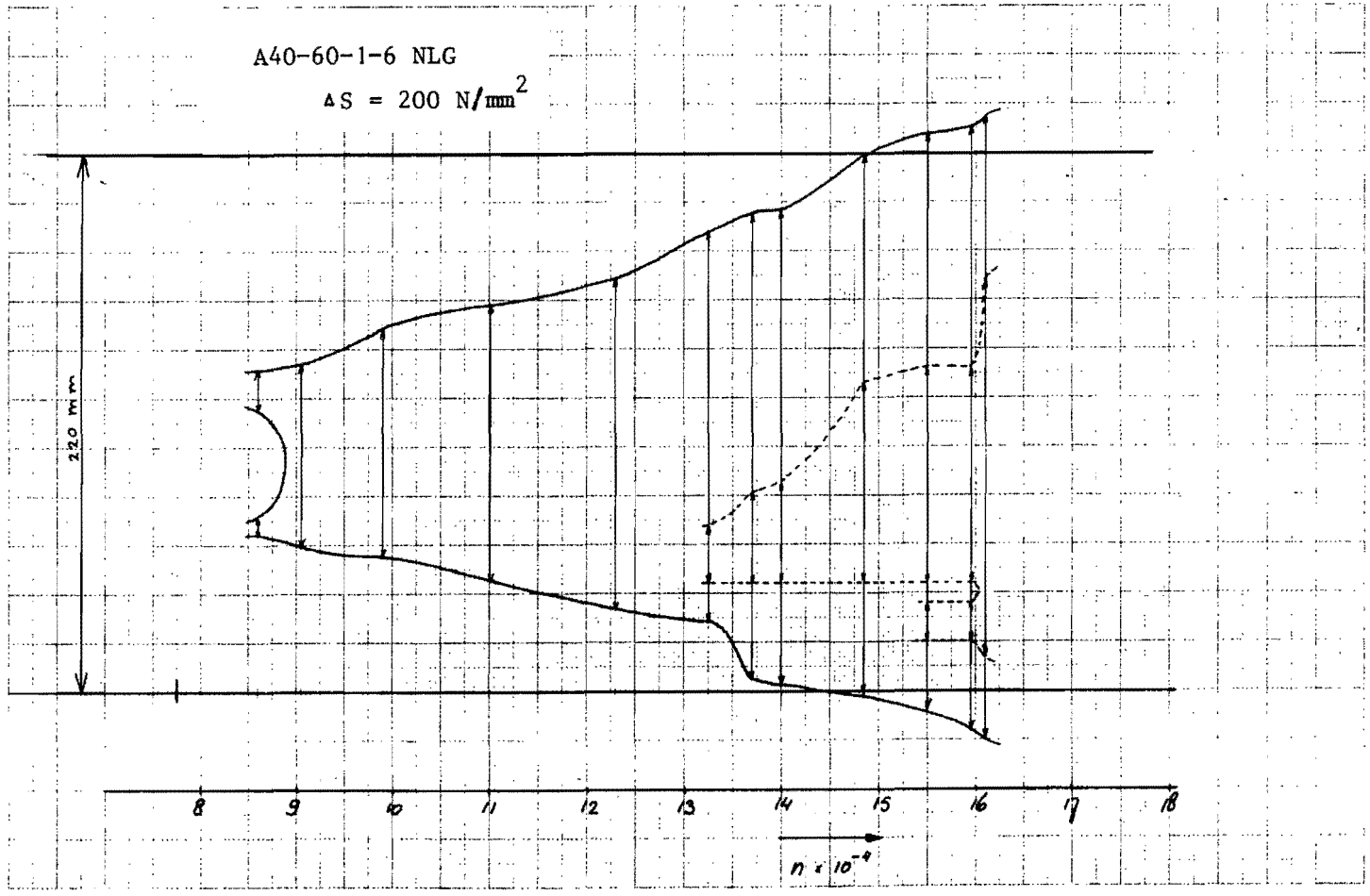

fig. 5f Continued

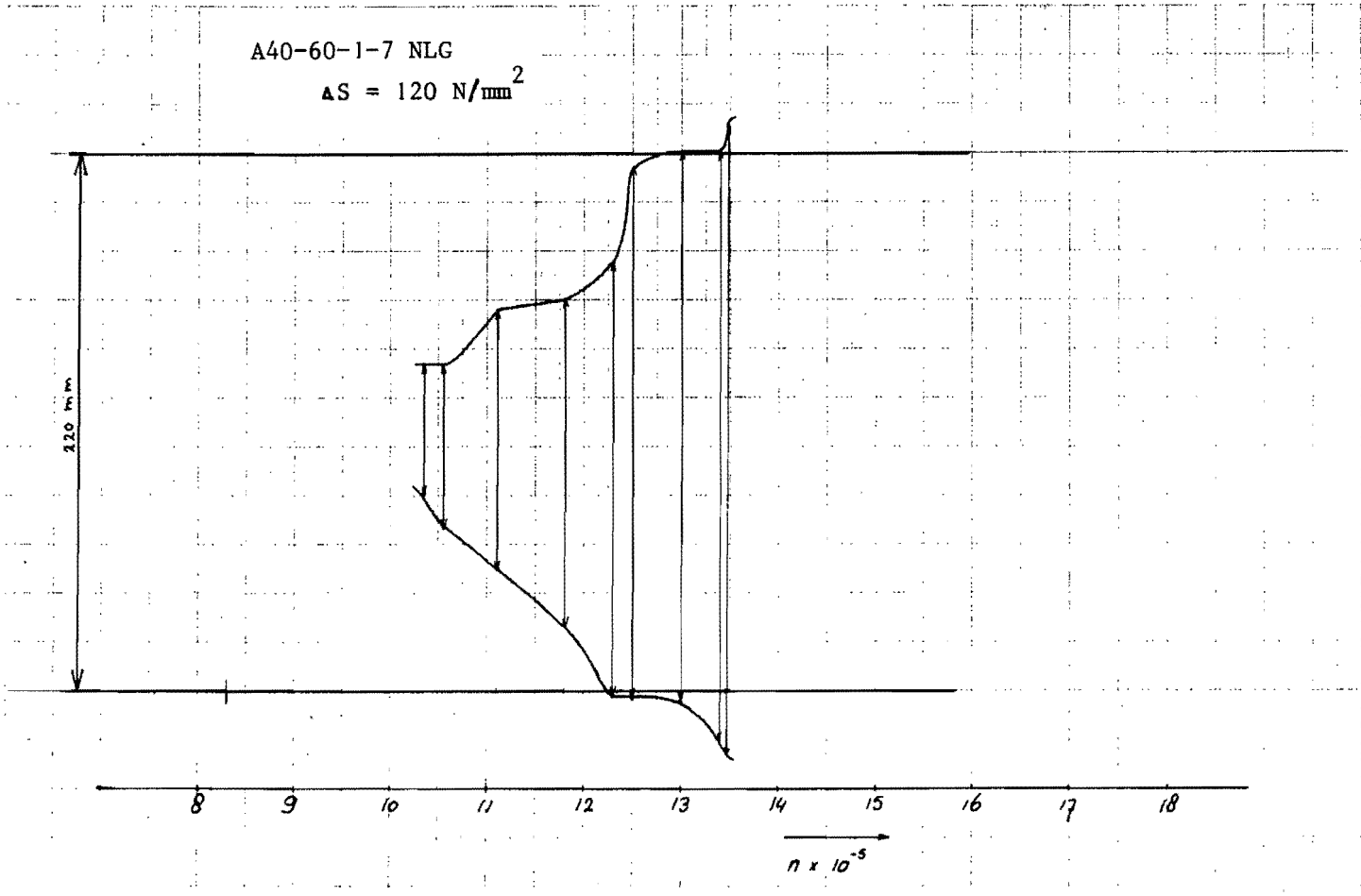

fig.5g Continued

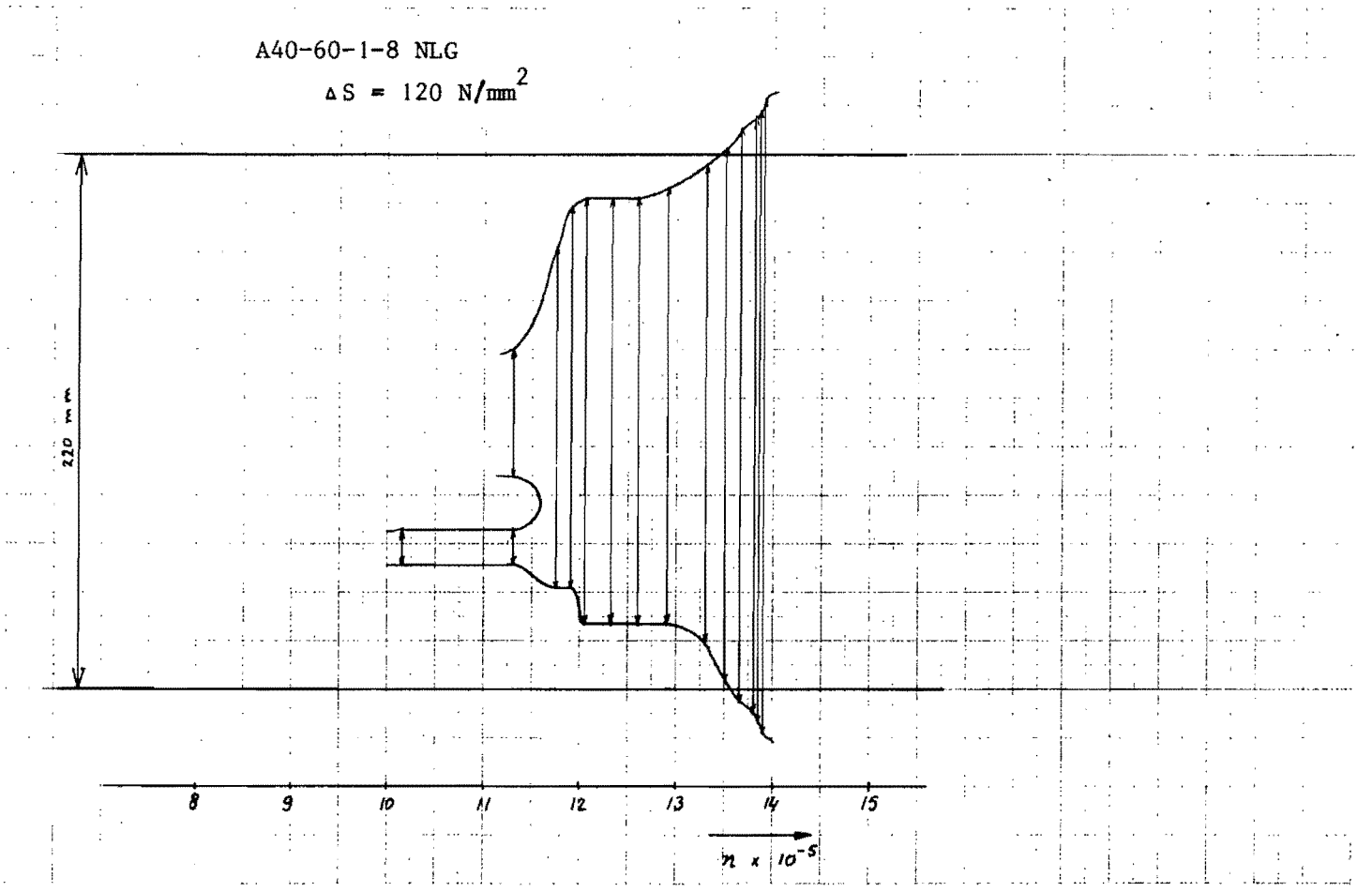

fig. 5h Continued

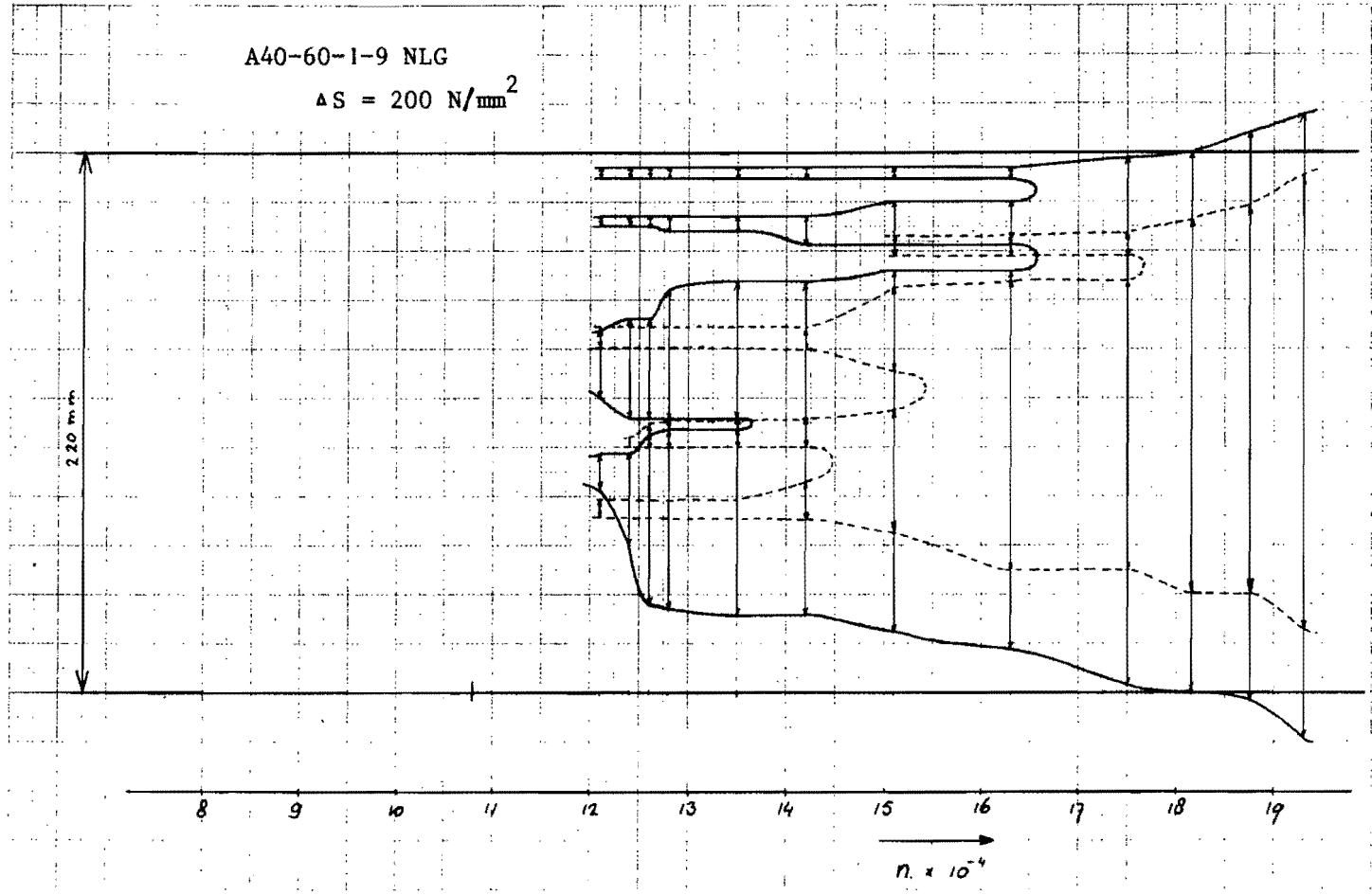

fig. 5i Continued

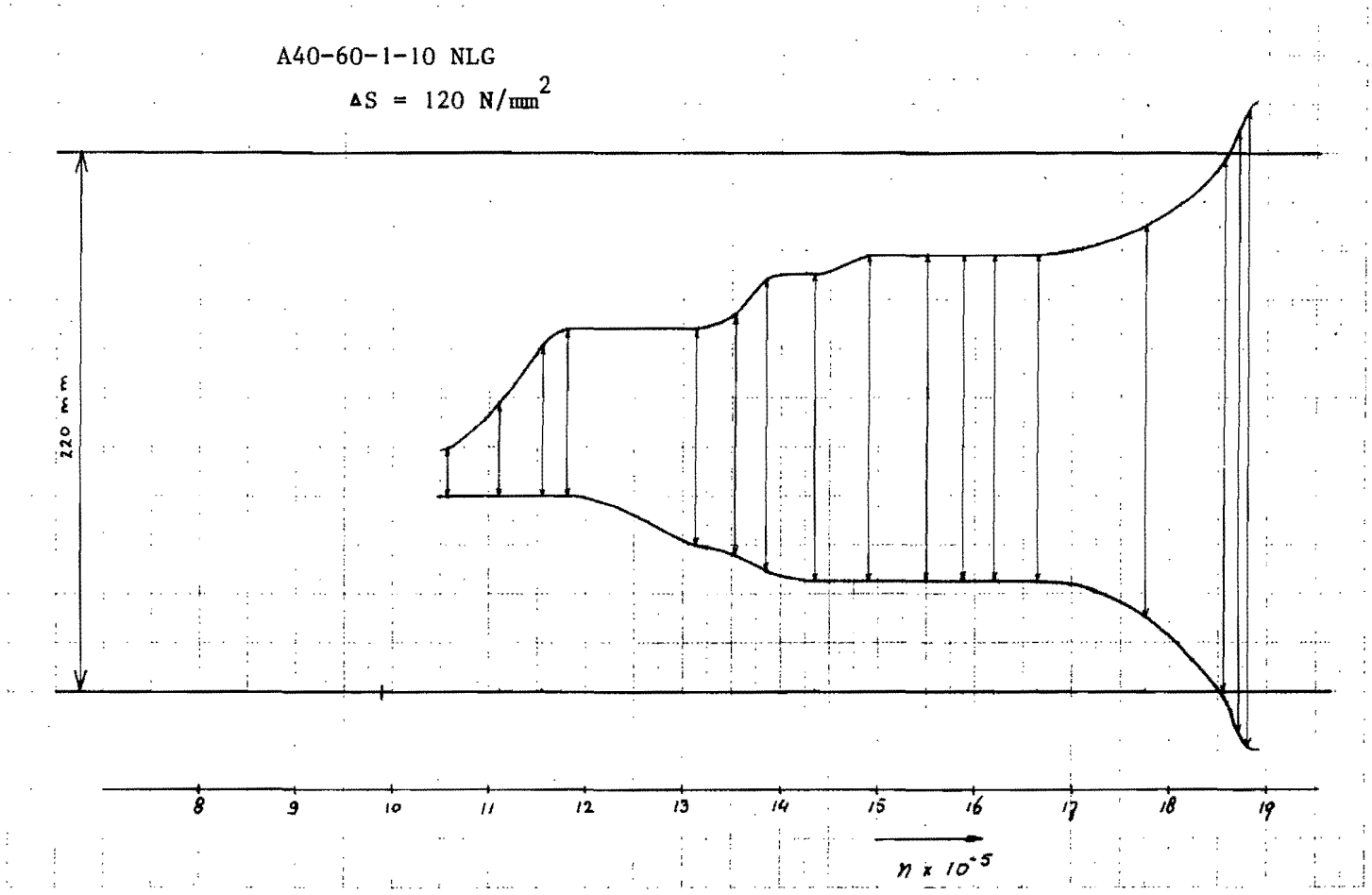
A40-60-1-10 NLG
ΔS = 120 N/mm²
220 mm
8
9
10
11
12
13
14
15
16
17
18
19
η x 10⁻⁵

fig. 5j End

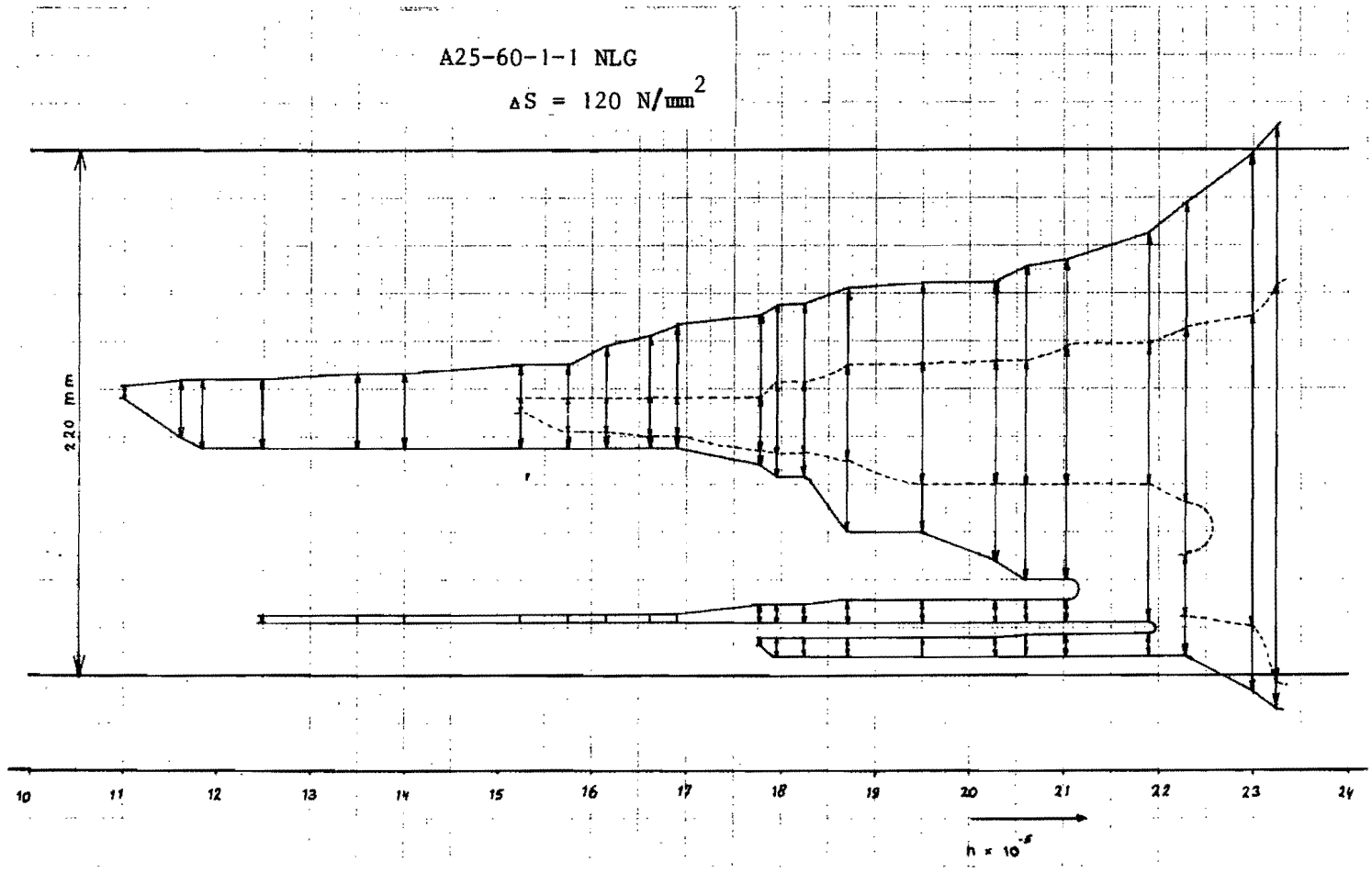

fig. 6a Crack growth measurements, specimens series A25

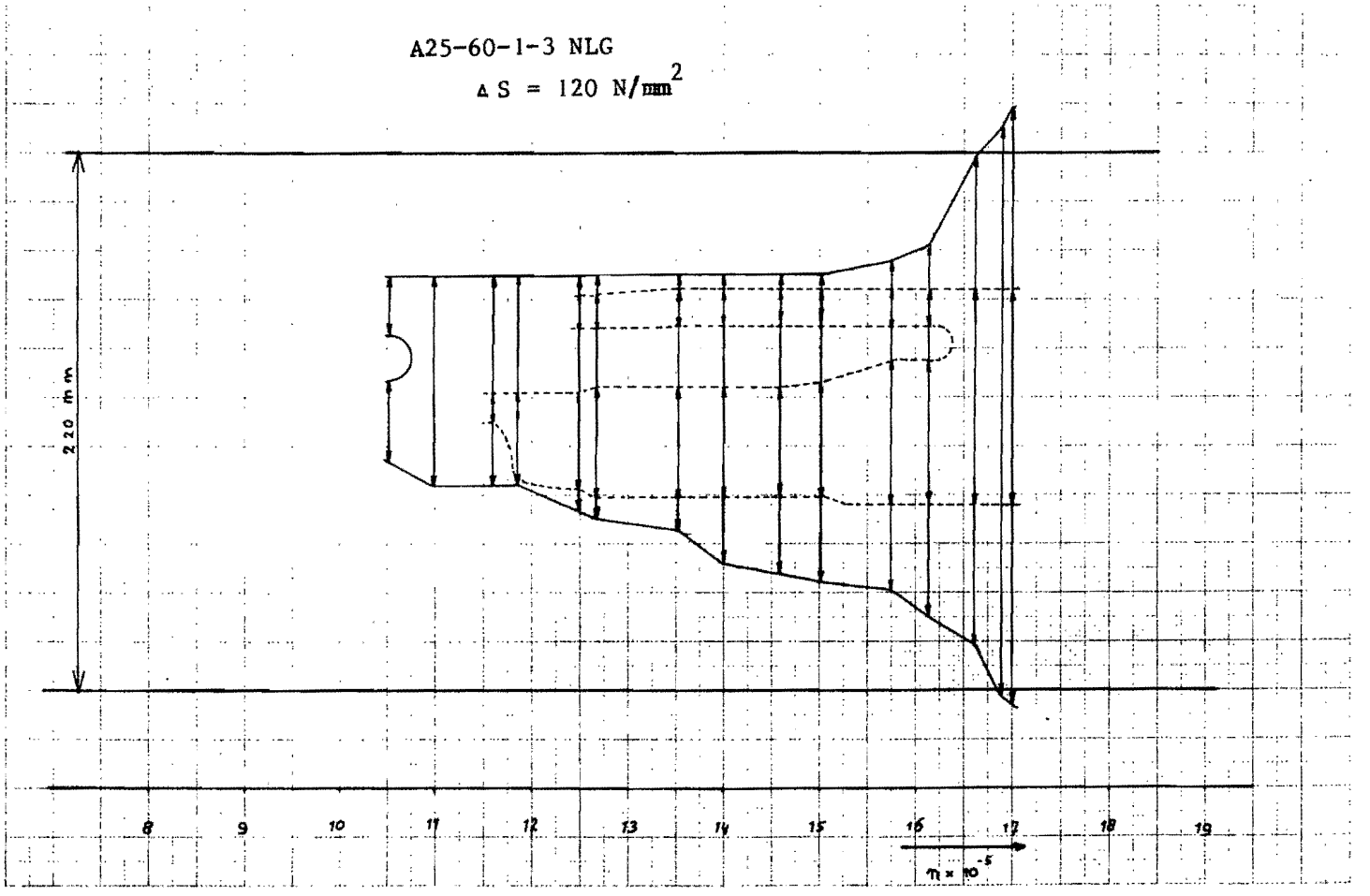

fig. 6b Continued

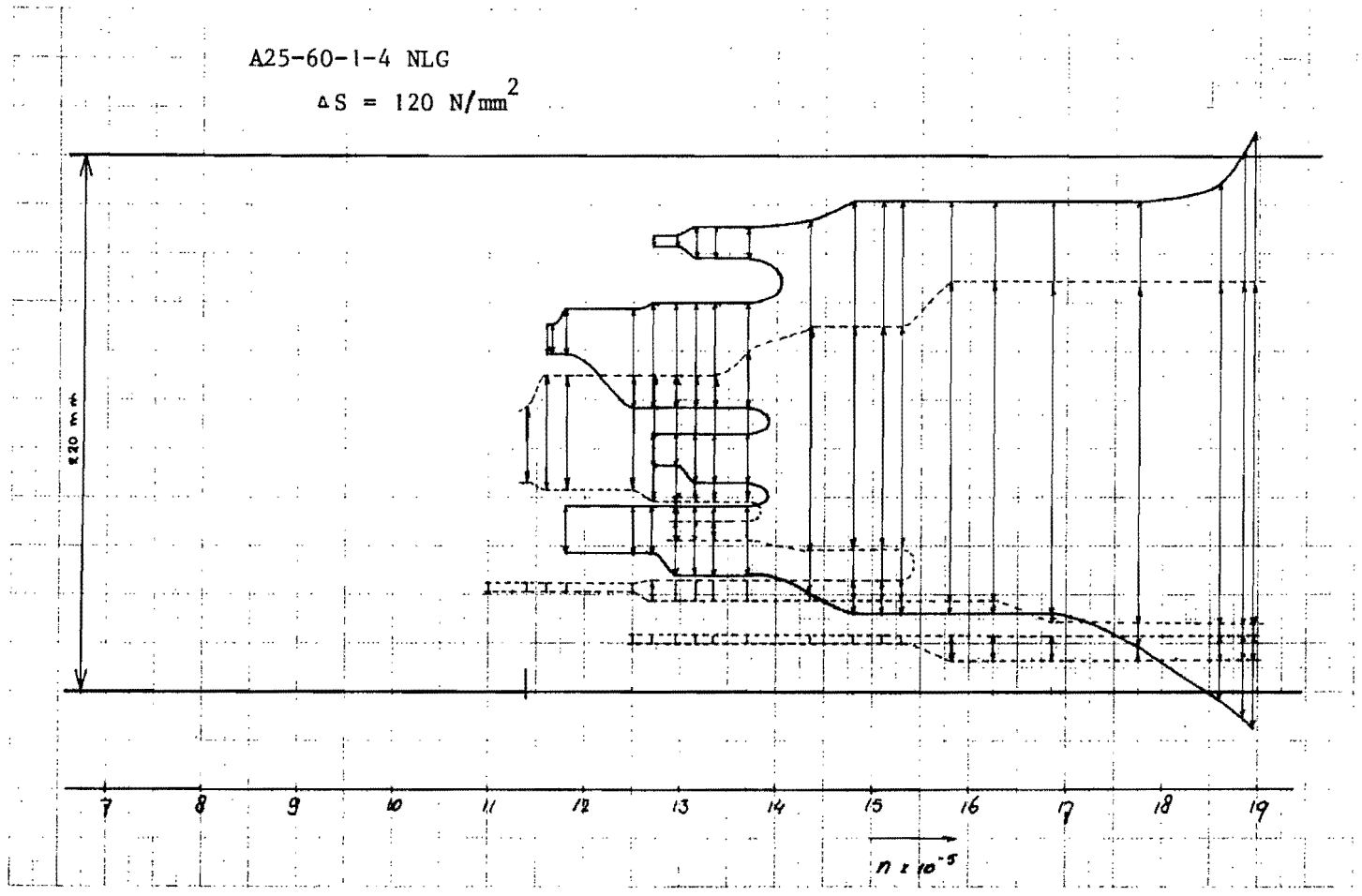

fig. 6c Continued

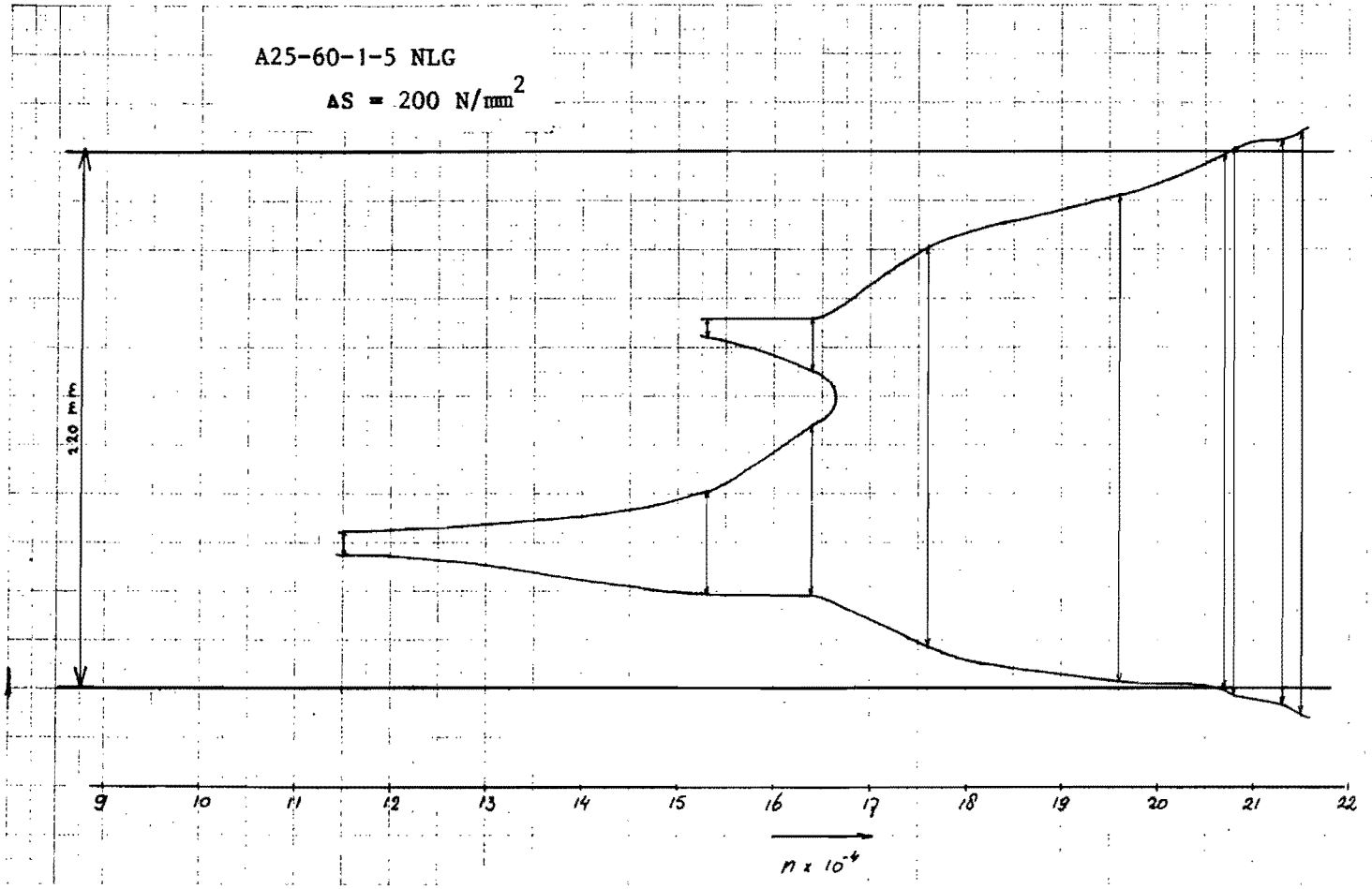

fig. 6d Continued

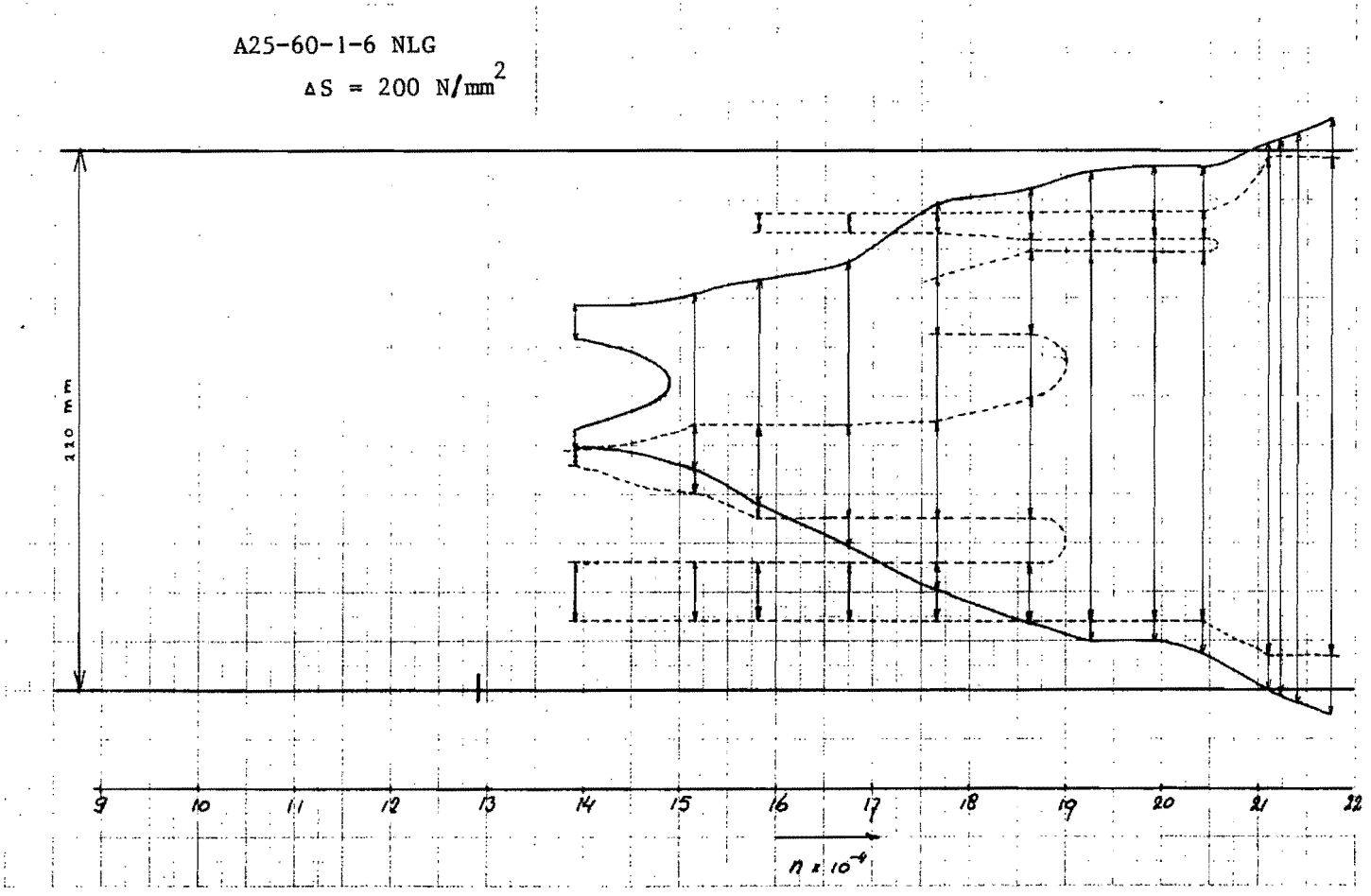

fig. 6e Continued

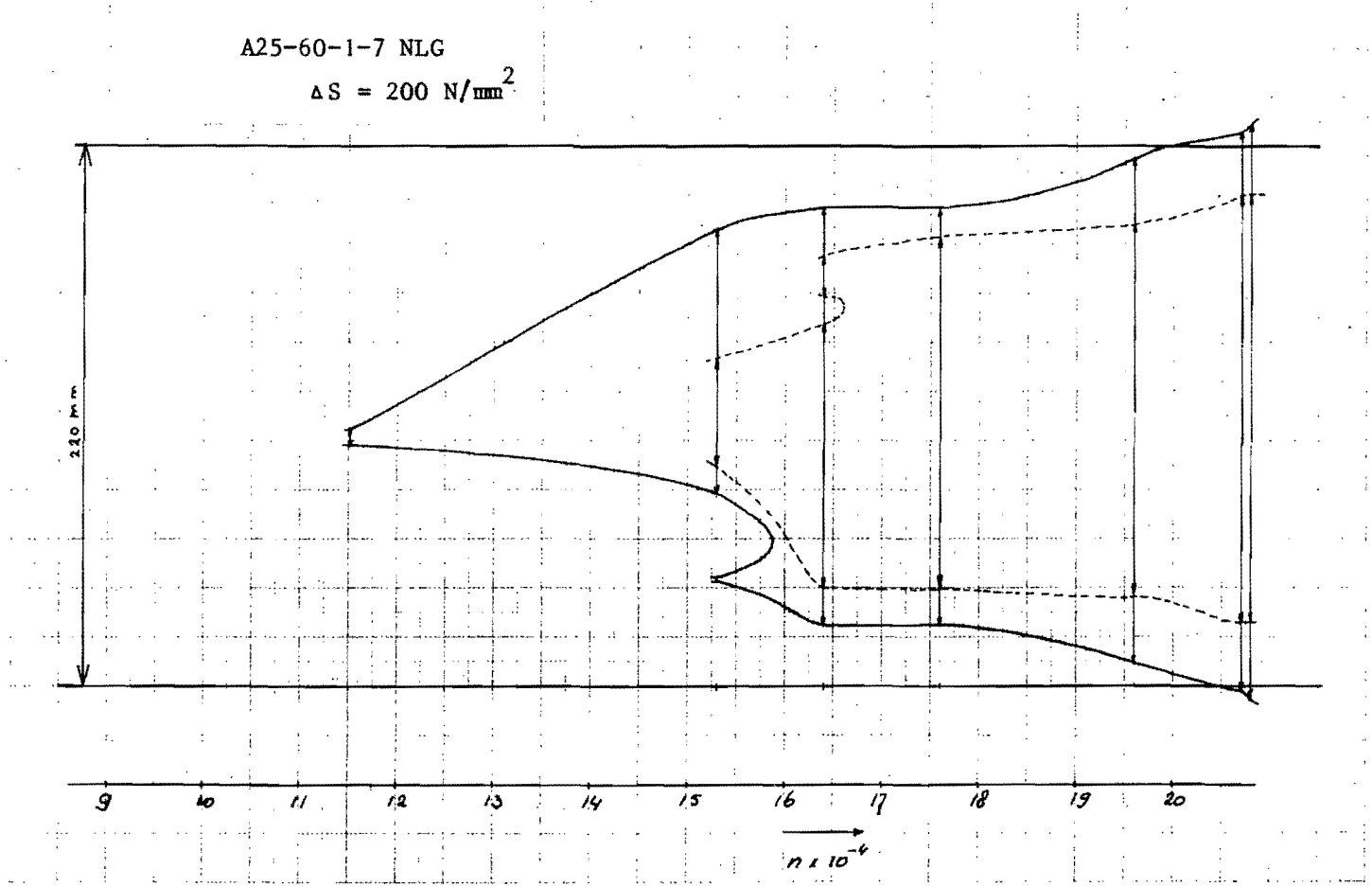

fig. 6f Continued

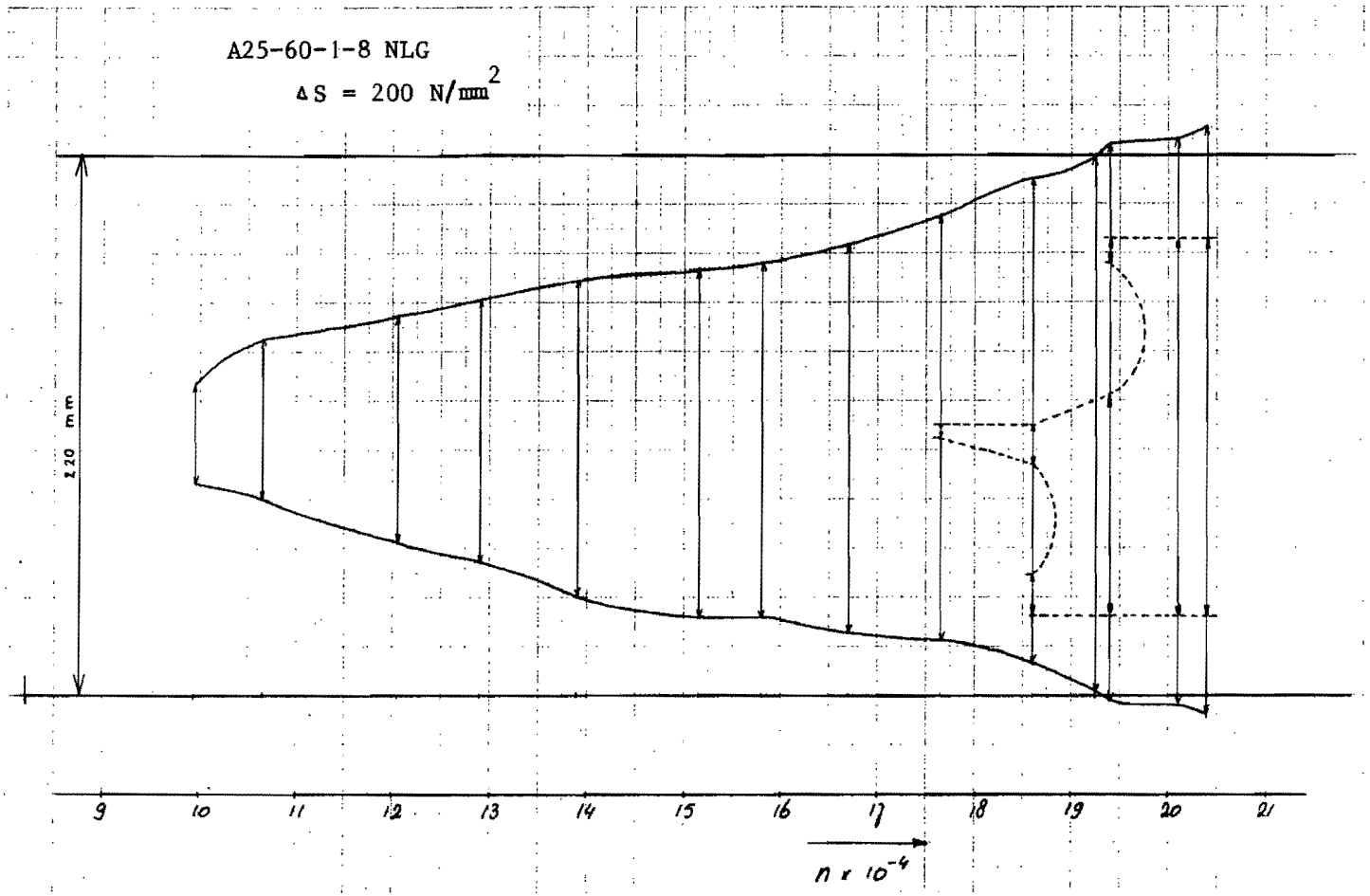

fig. 6g Continued

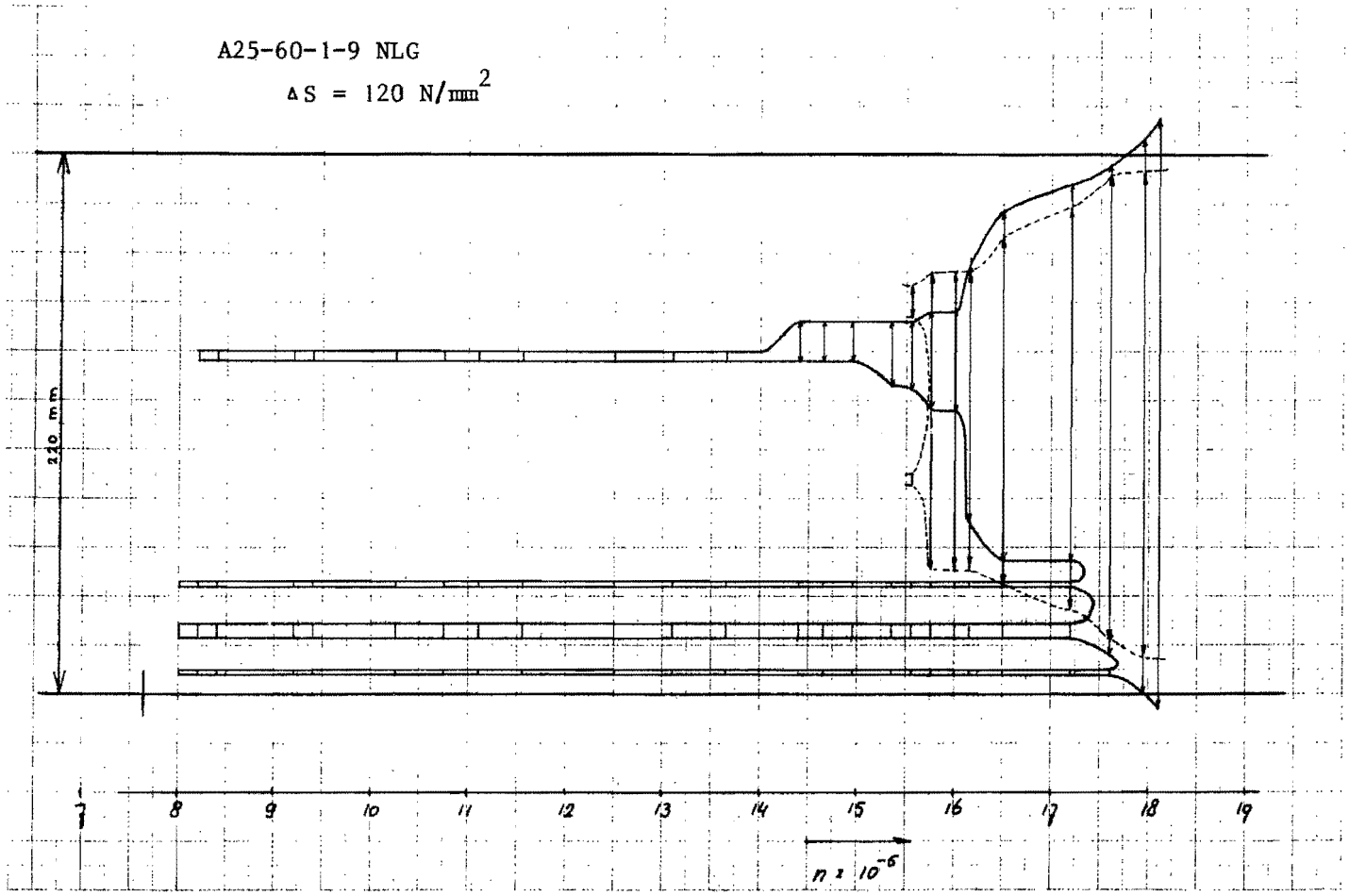

fig. 6h Continued

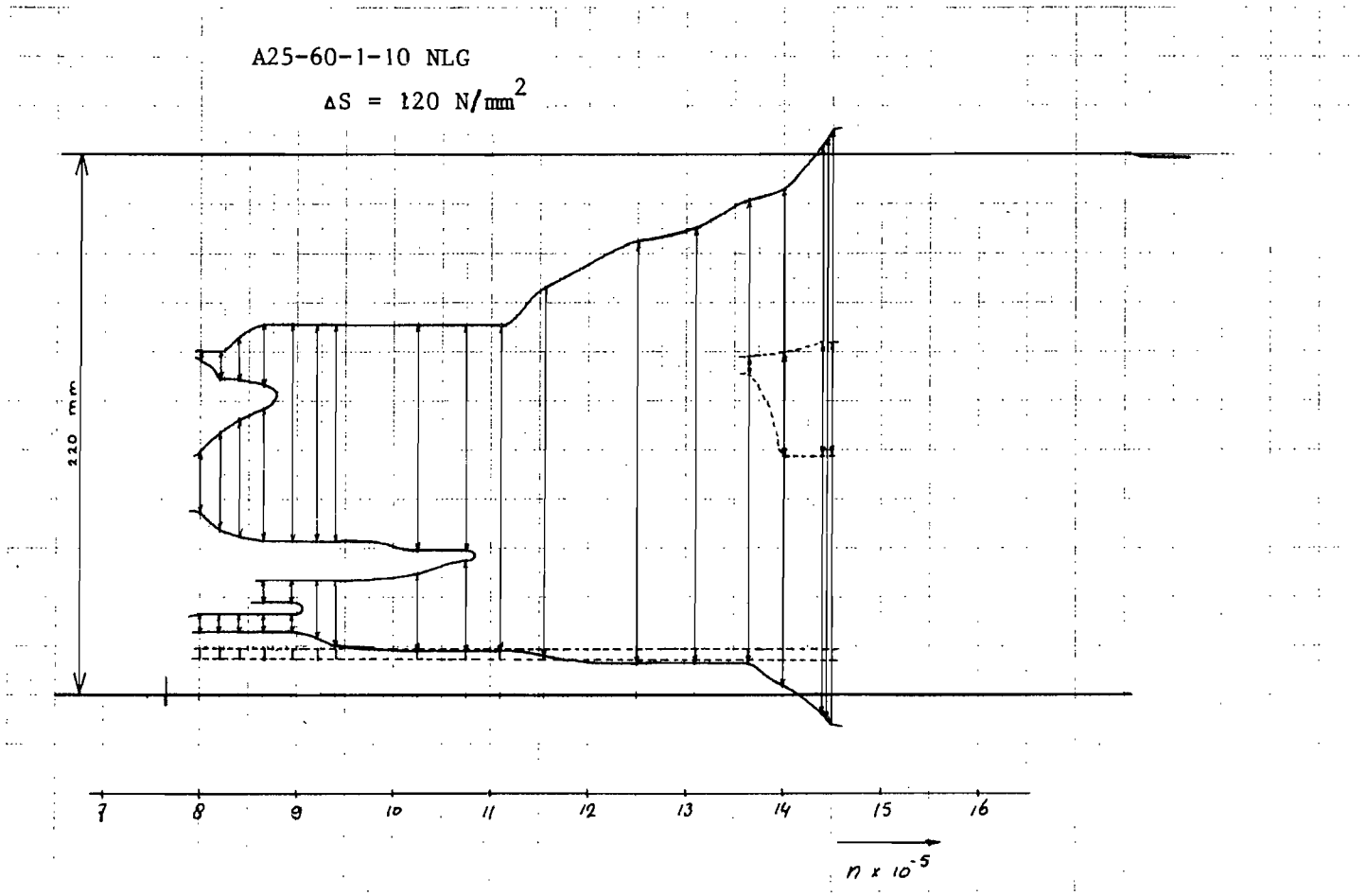

fig. 6i Continued

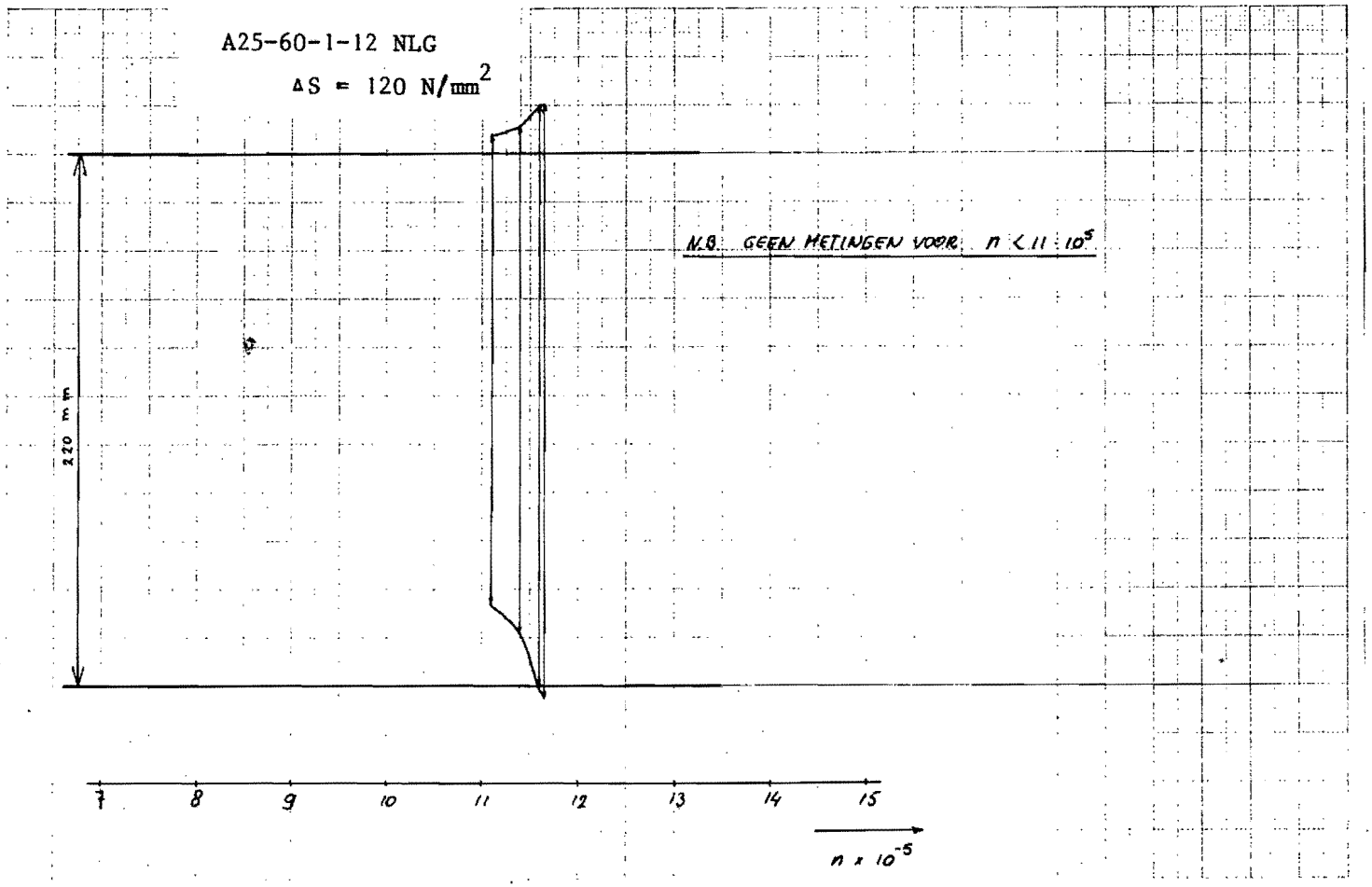
A25-60-1-12 NLG
ΔS = 120 N/mm²
N.B. GEEN METINGEN VOOR n < 11 · 10⁵
ε
220
7
8
9
10
11
12
13
14
15
n × 10⁻⁵

fig. 6j End

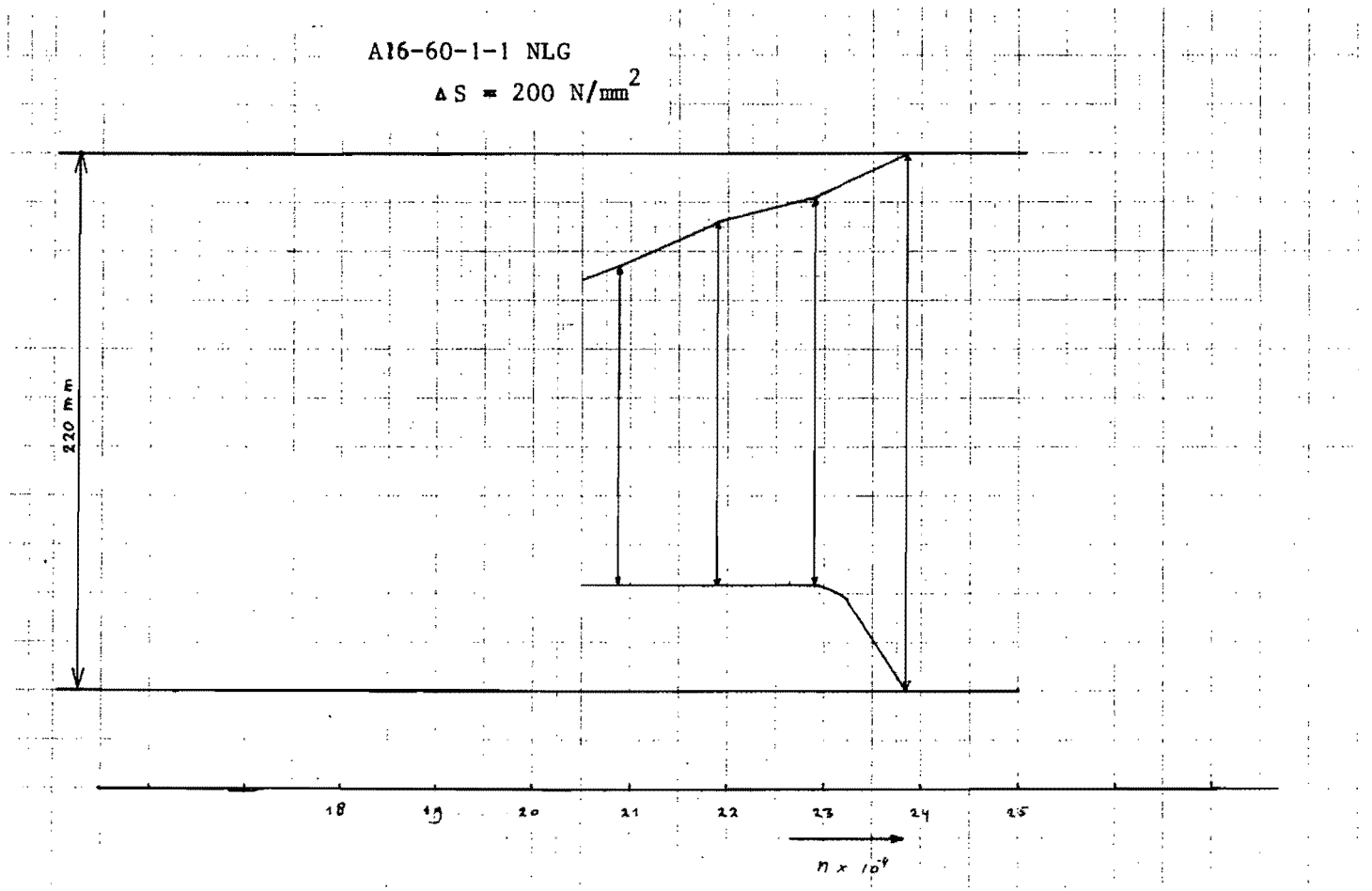

fig. 7a Crack growth measurements, specimens series A16

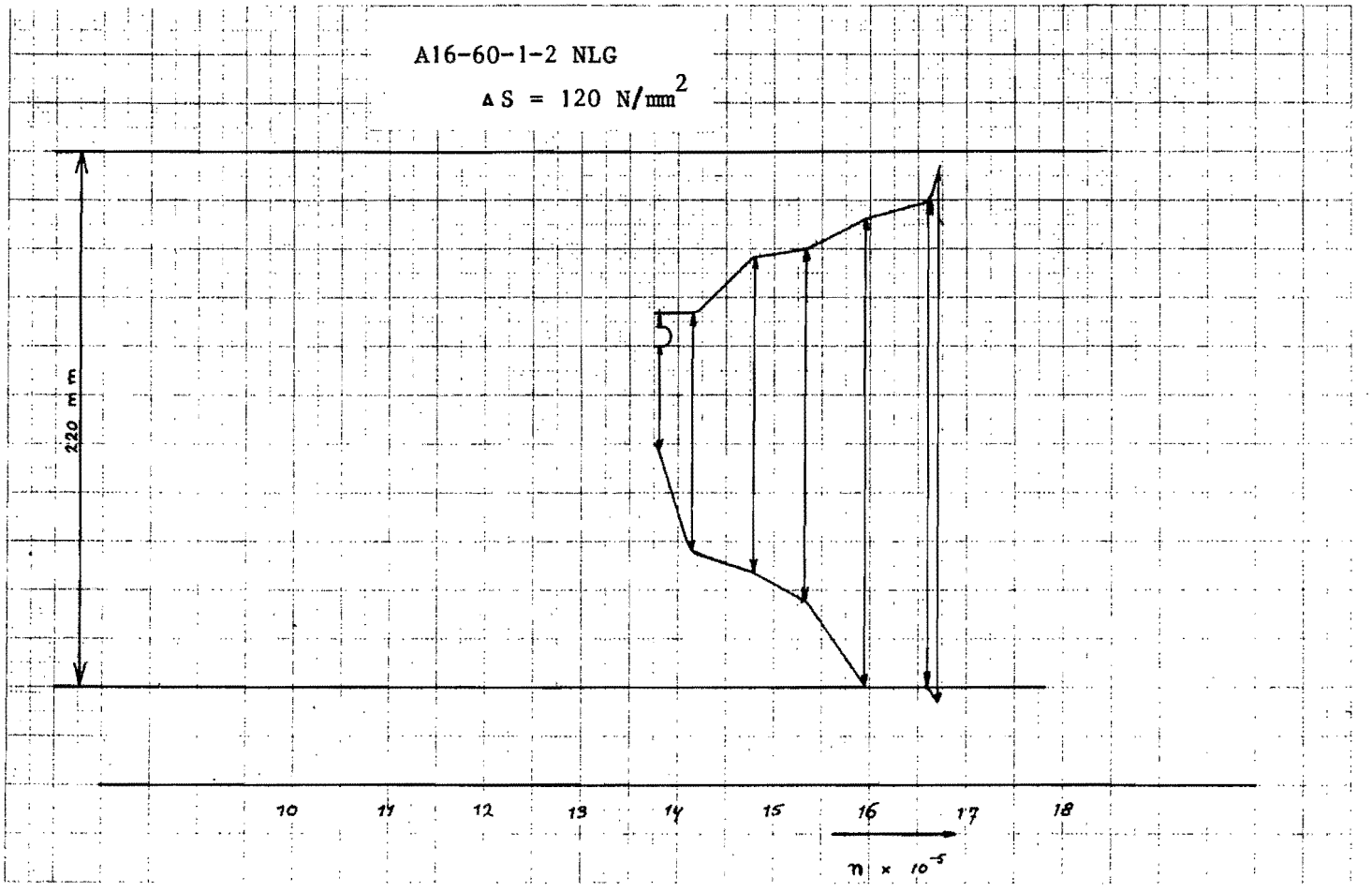

fig. 7b Continued

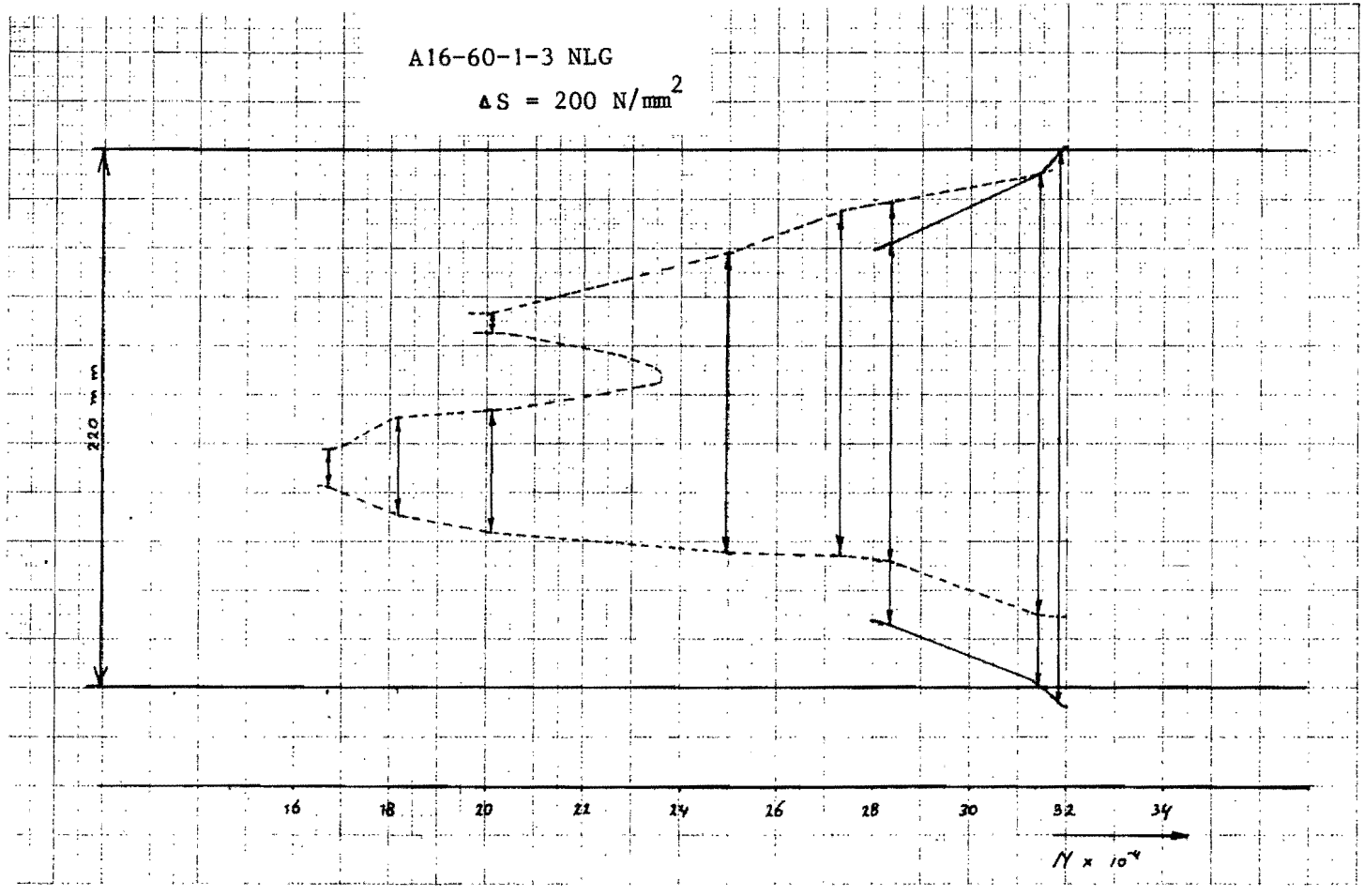

fig. 7c Continued

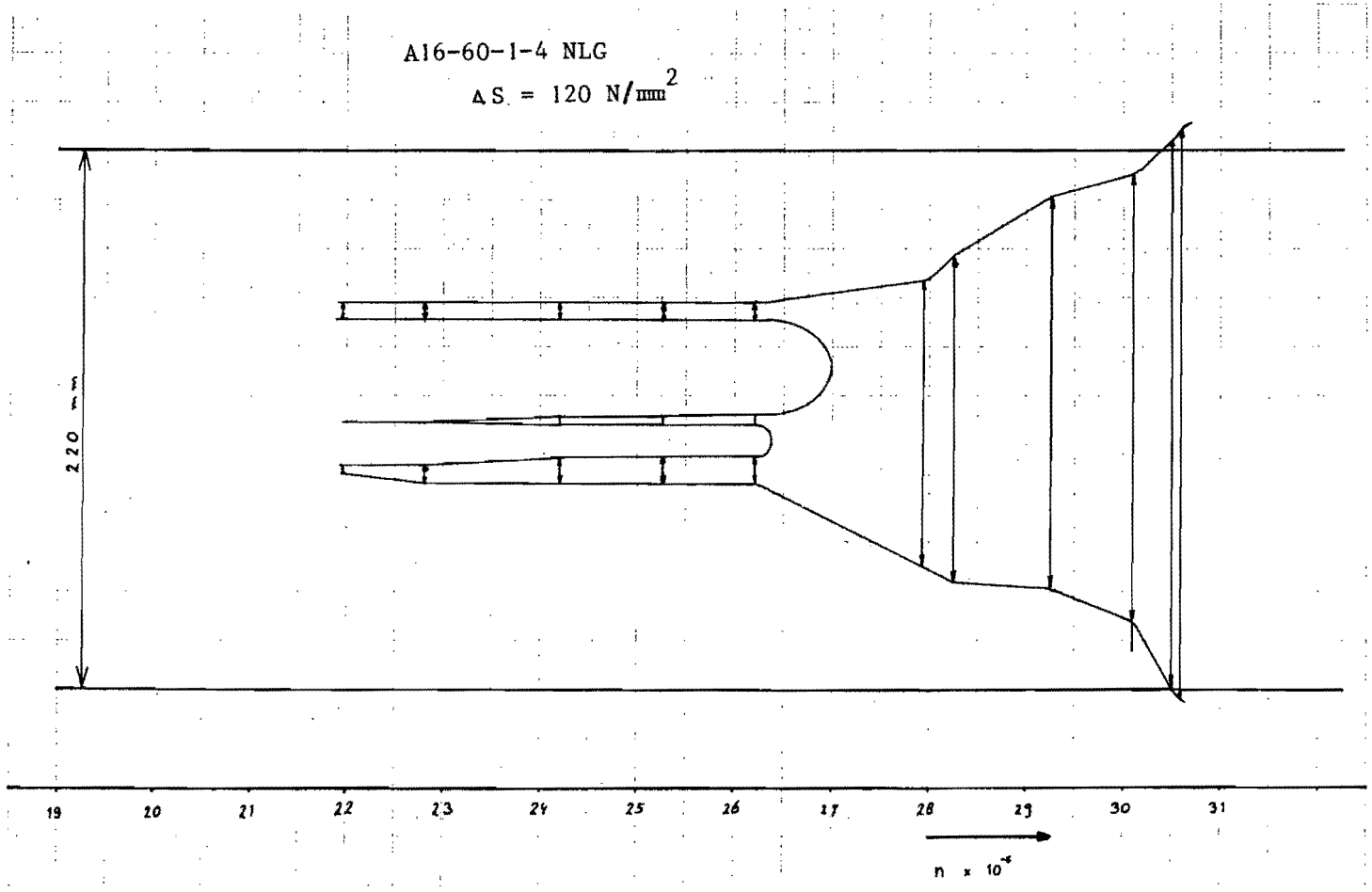

fig. 7d Continued

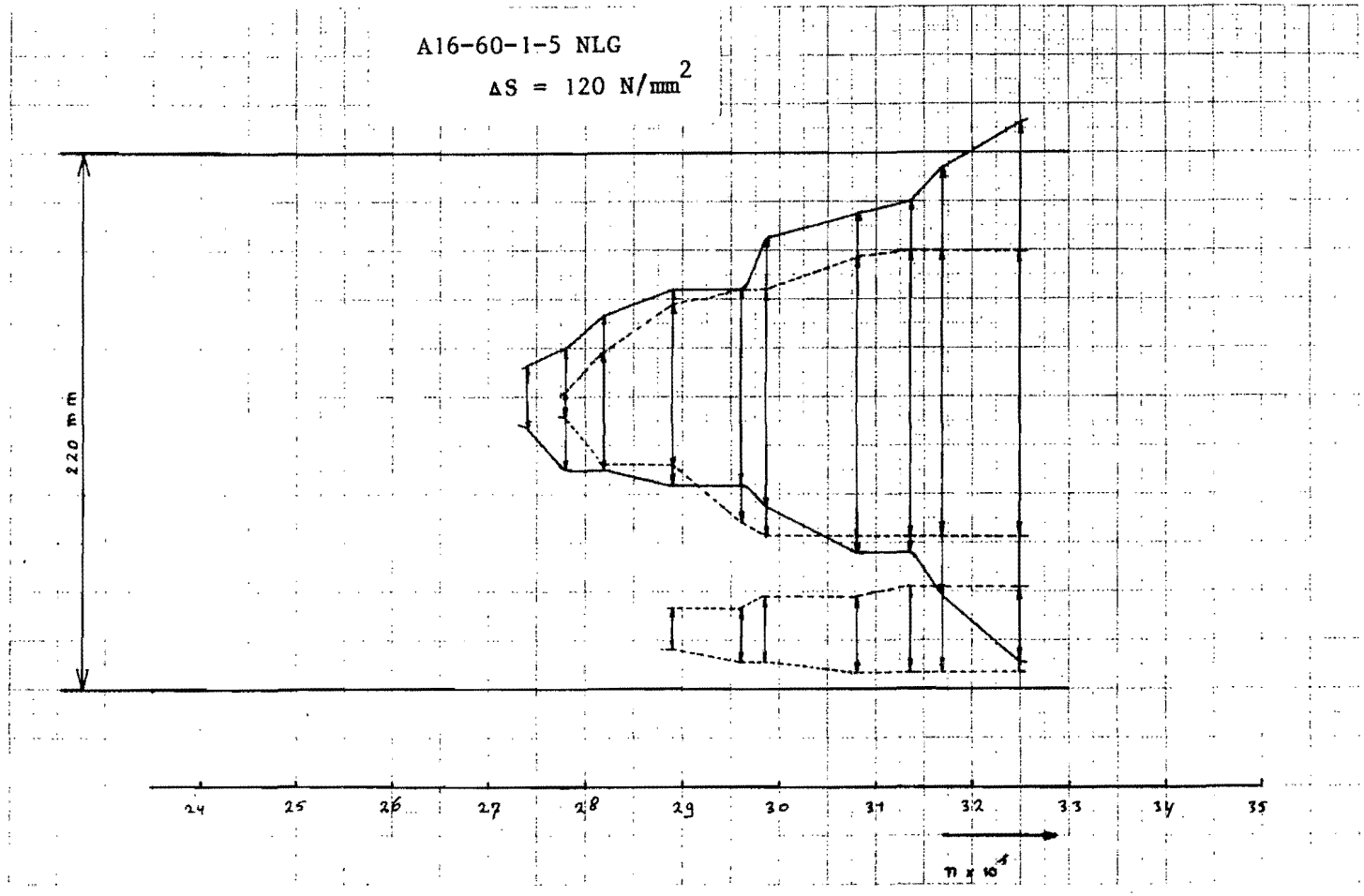

fig.7e Continued

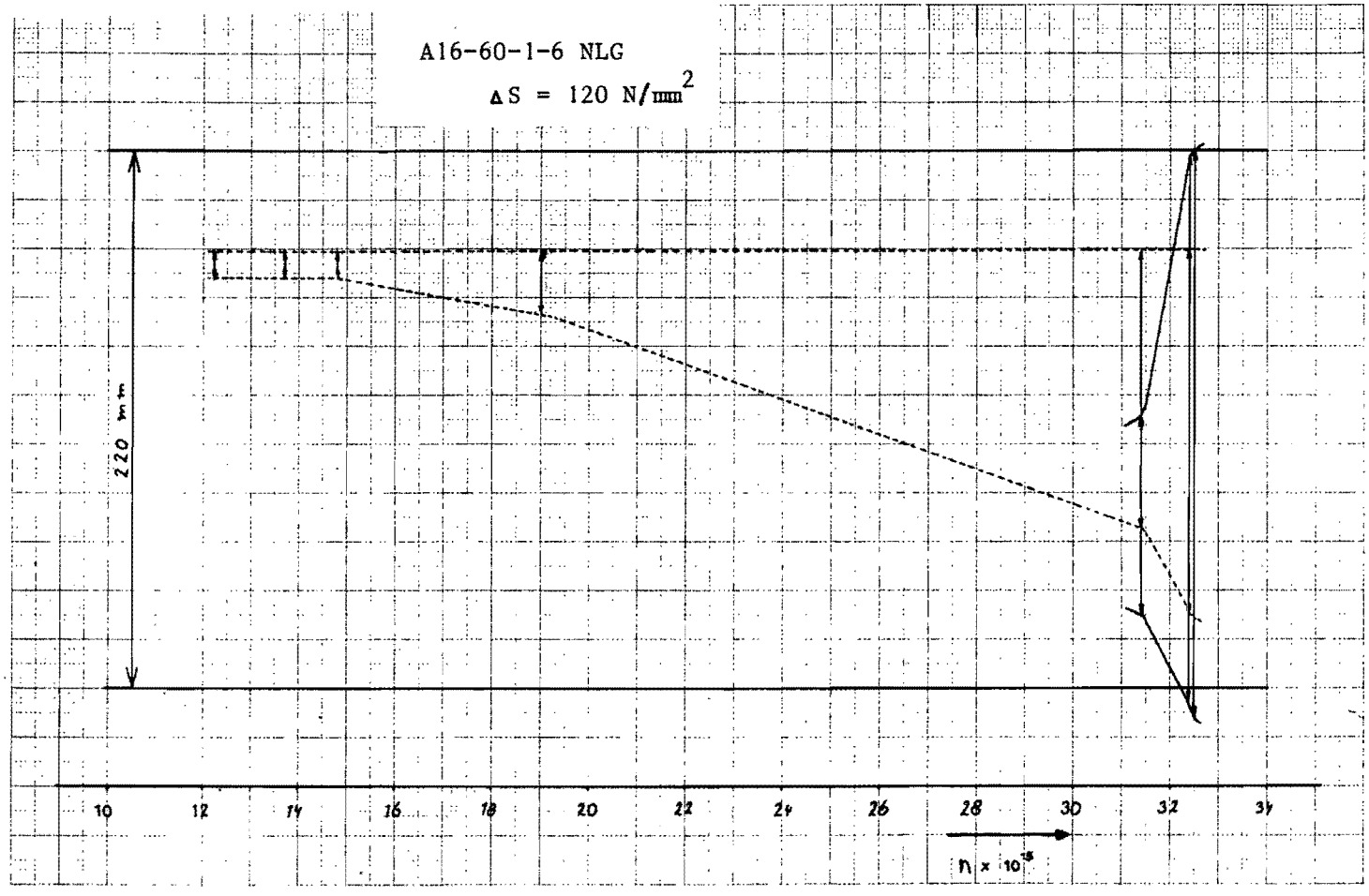

fig. 7f Continued

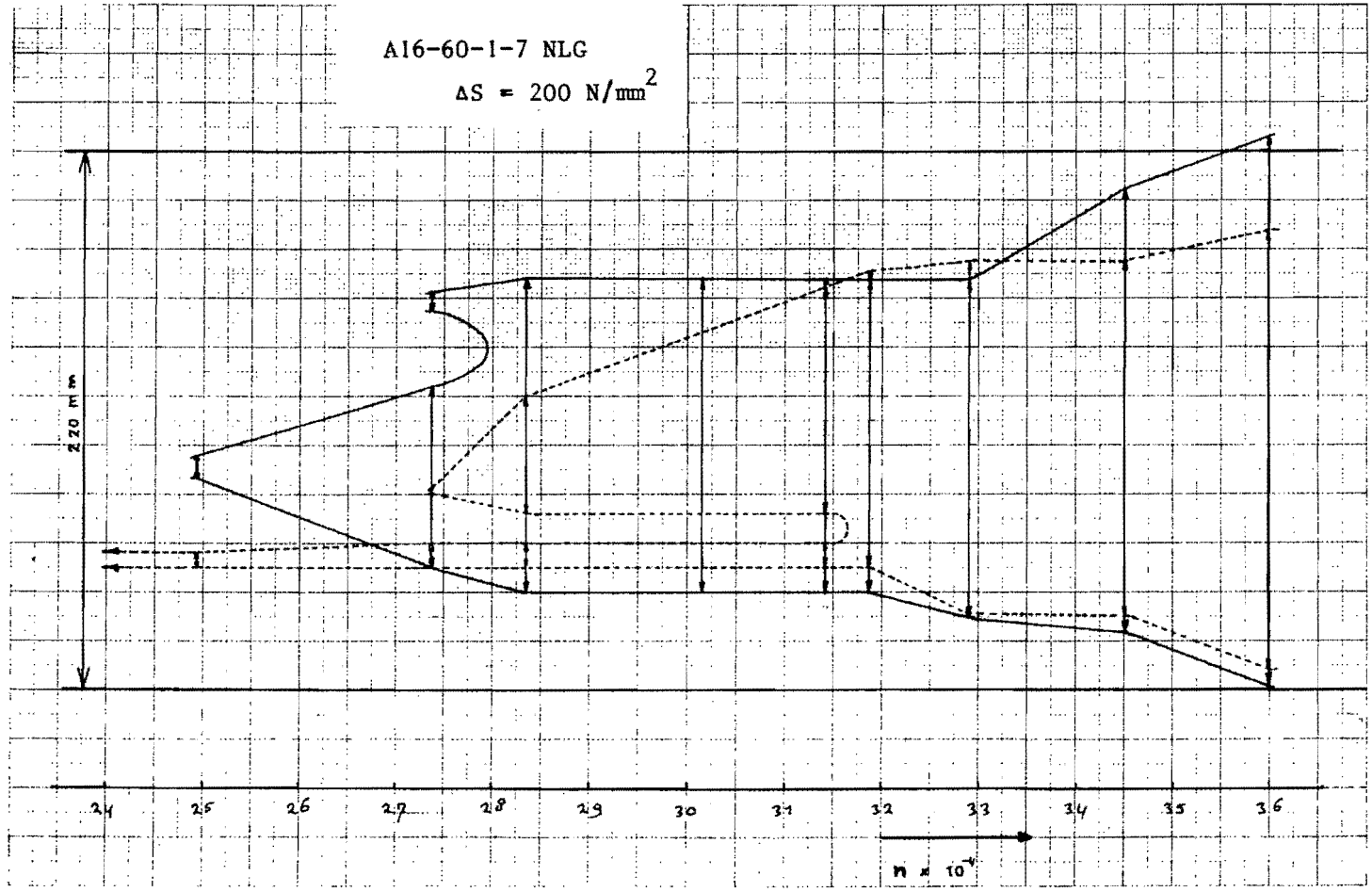

fig. 7g Continued

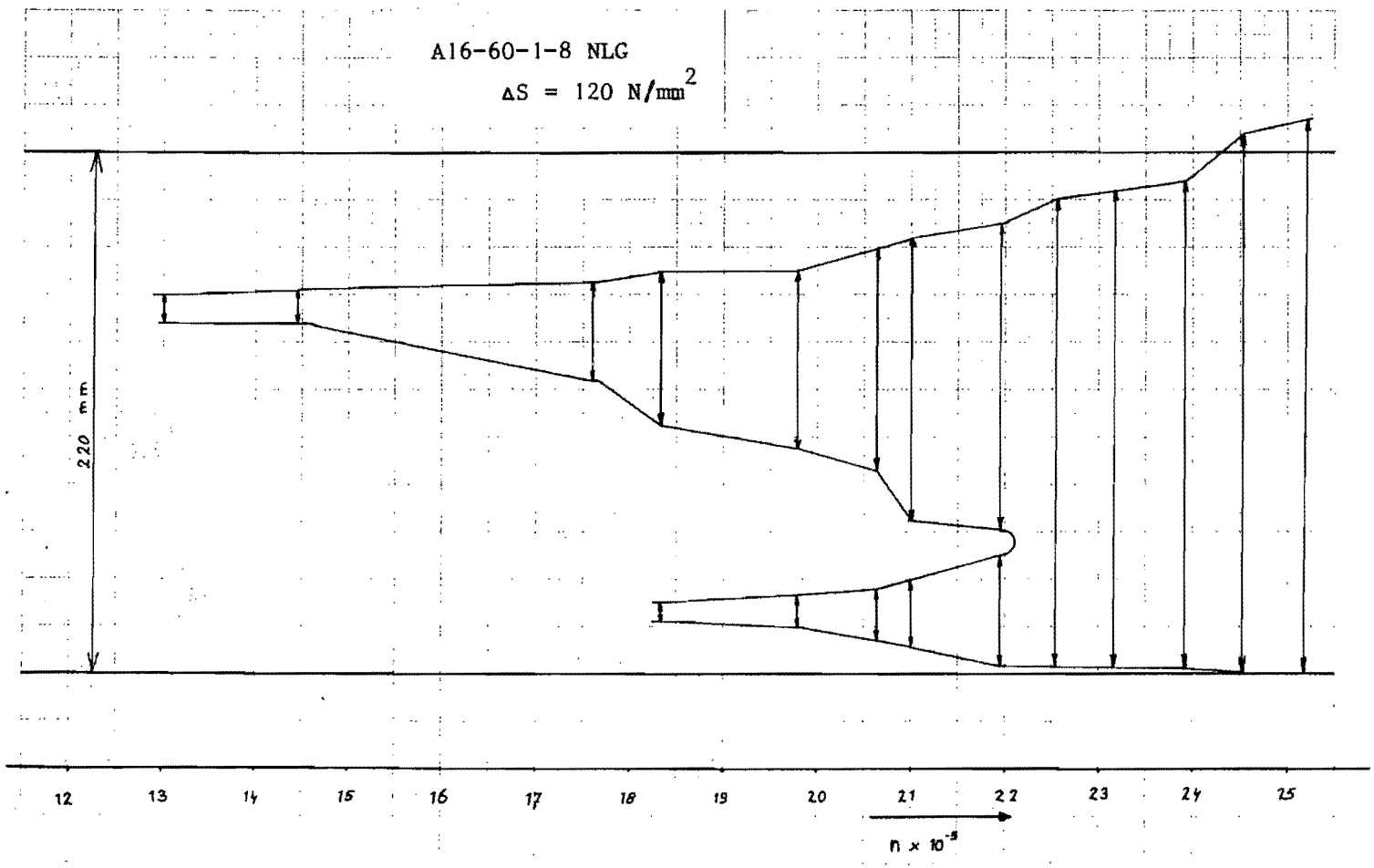

fig. 7h Continued

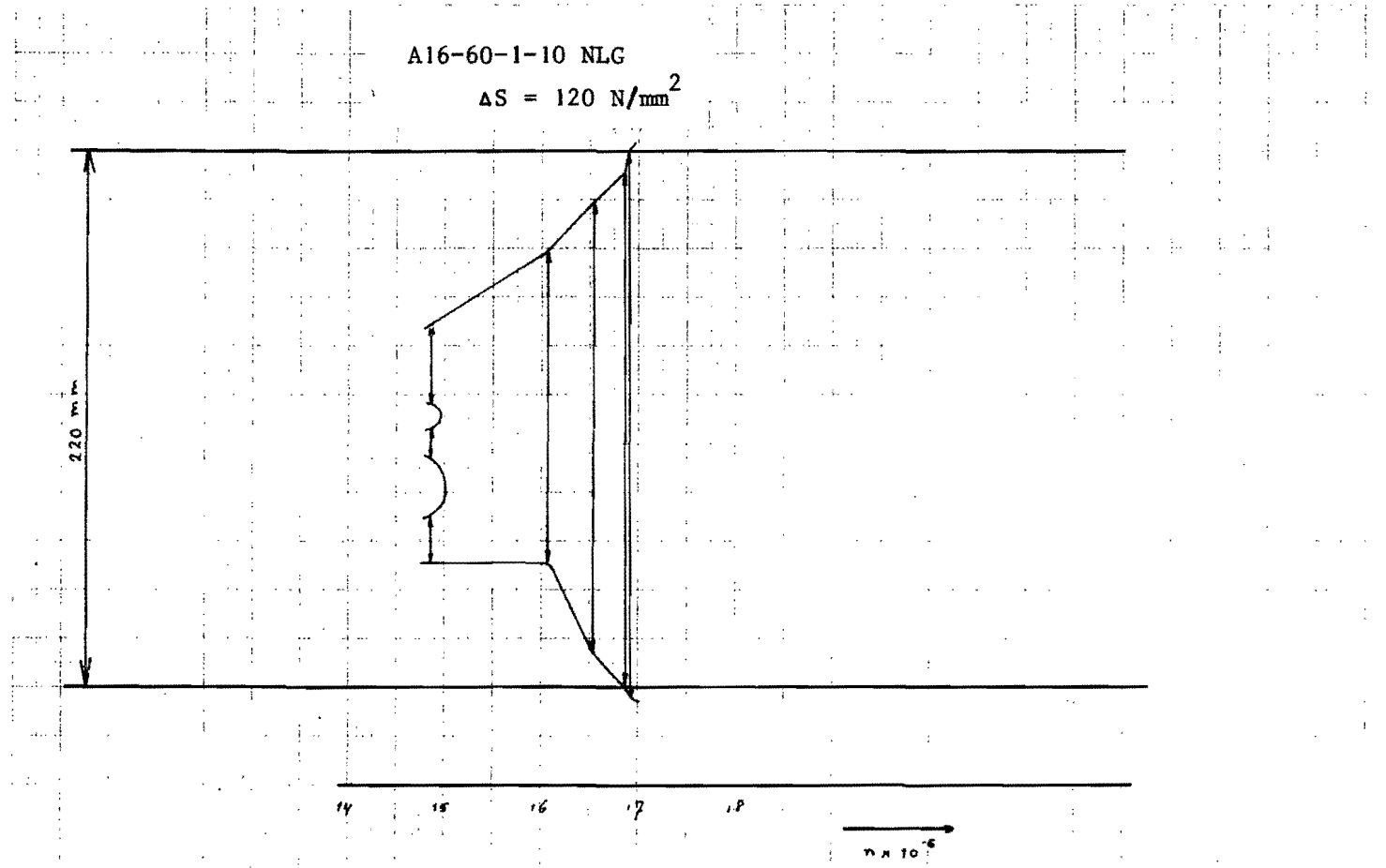

fig. 7j Continued

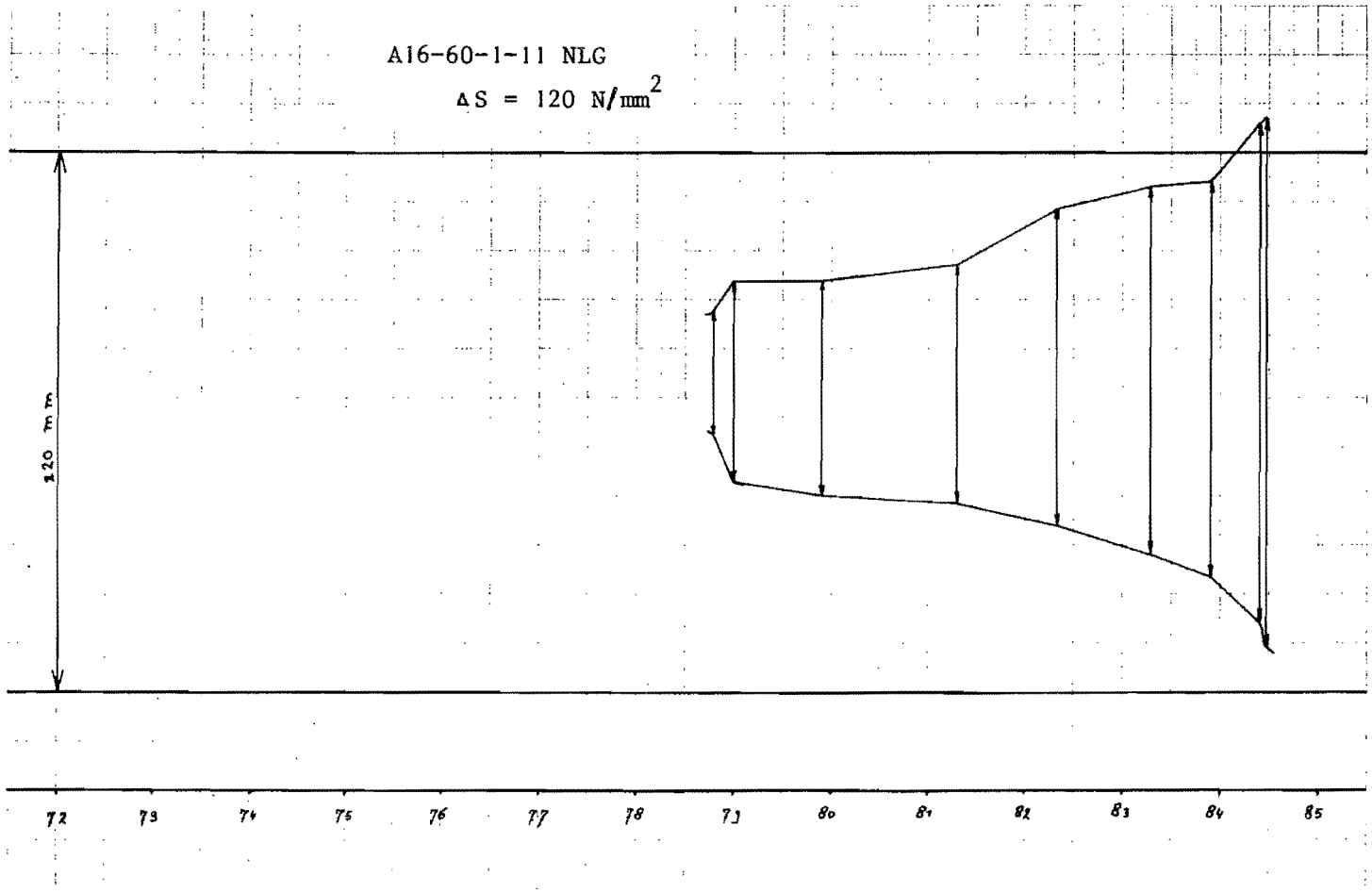
A16-60-1-11 NLG
ΔS = 120 N/mm²
120 mm
72
73
74
75
76
77
78
79
80
81
82
83
84
85

fig. 7k End

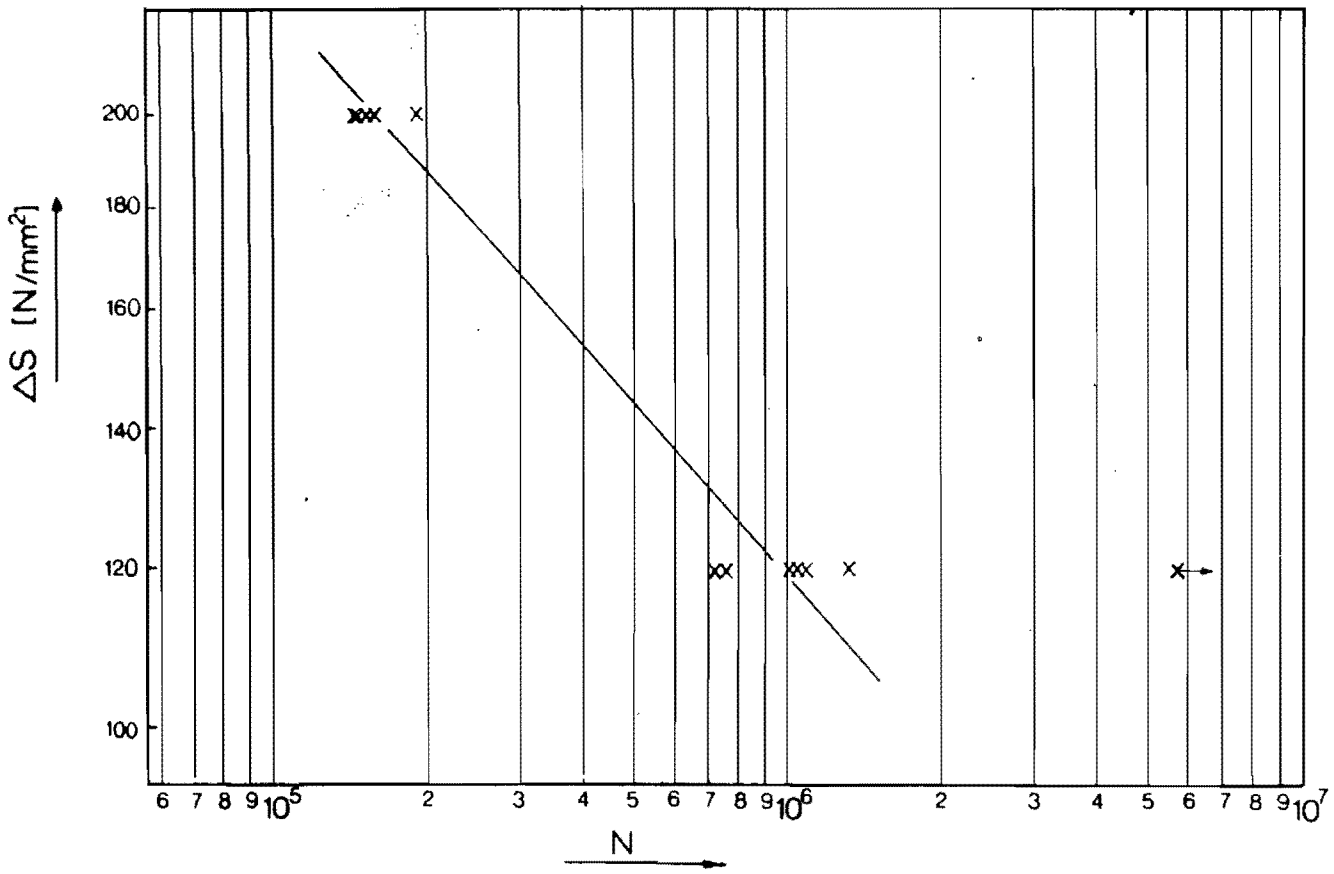

fig. 8 Endurances Series A70

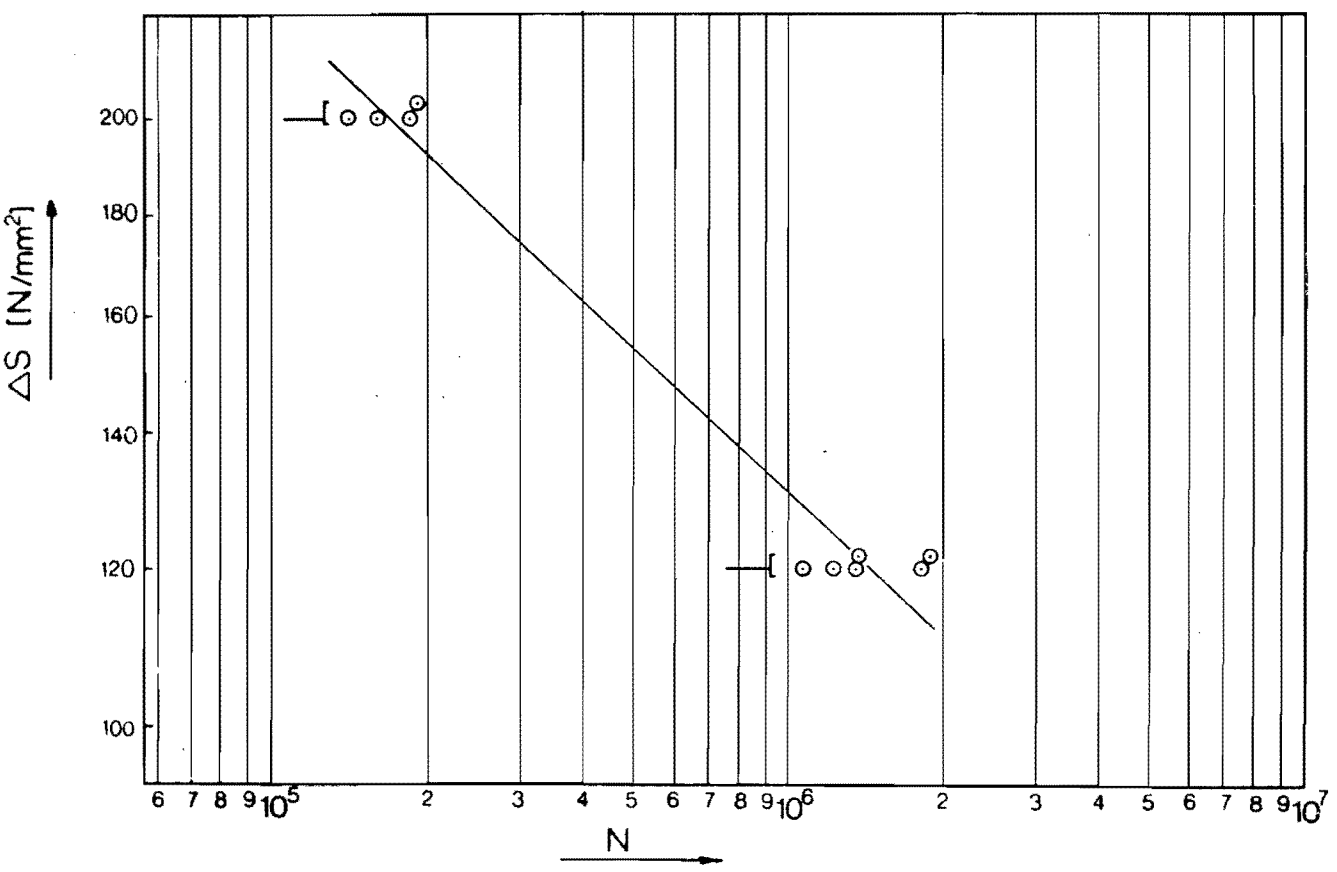

fig. 9 Endurances Series A40

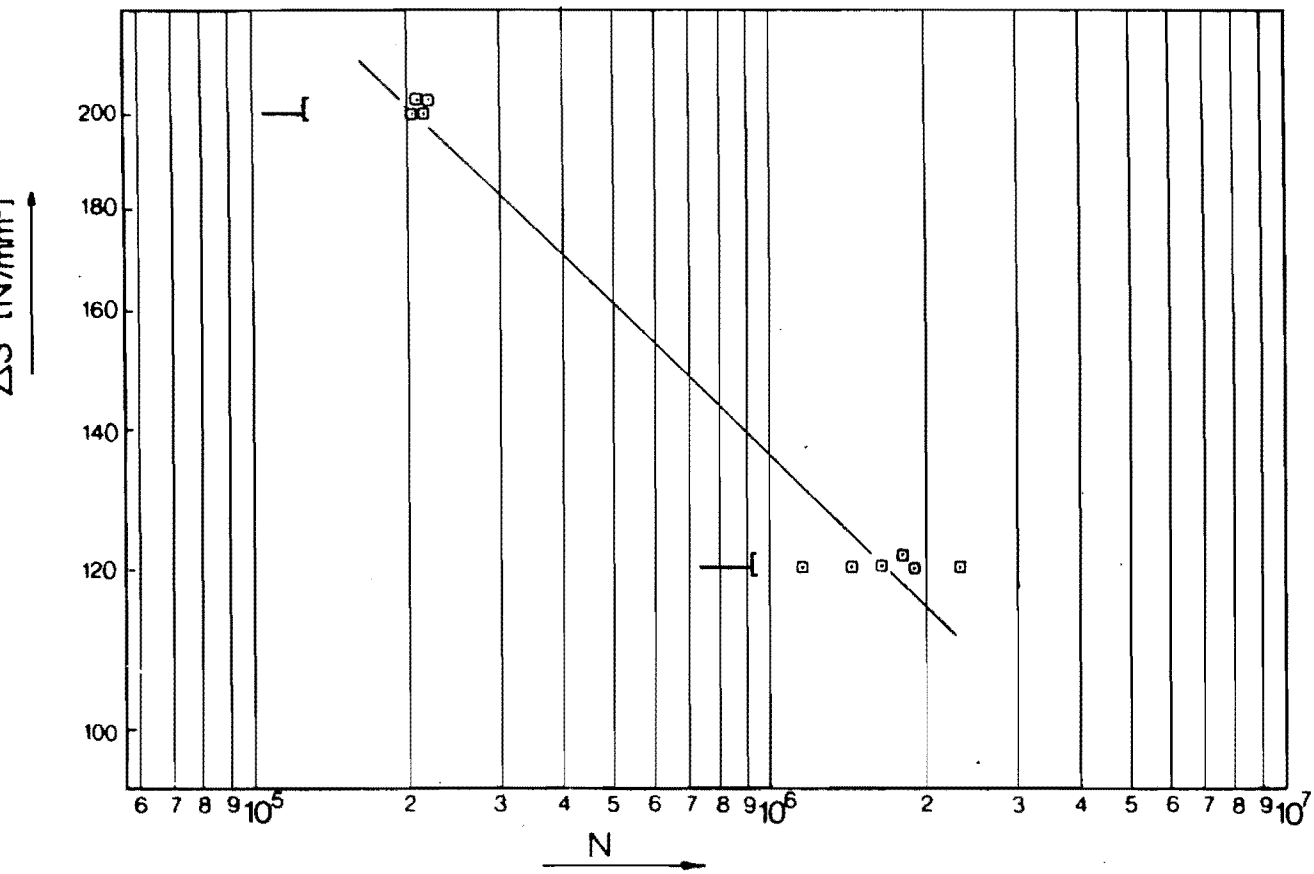

fig. 10 Endurances Series A25

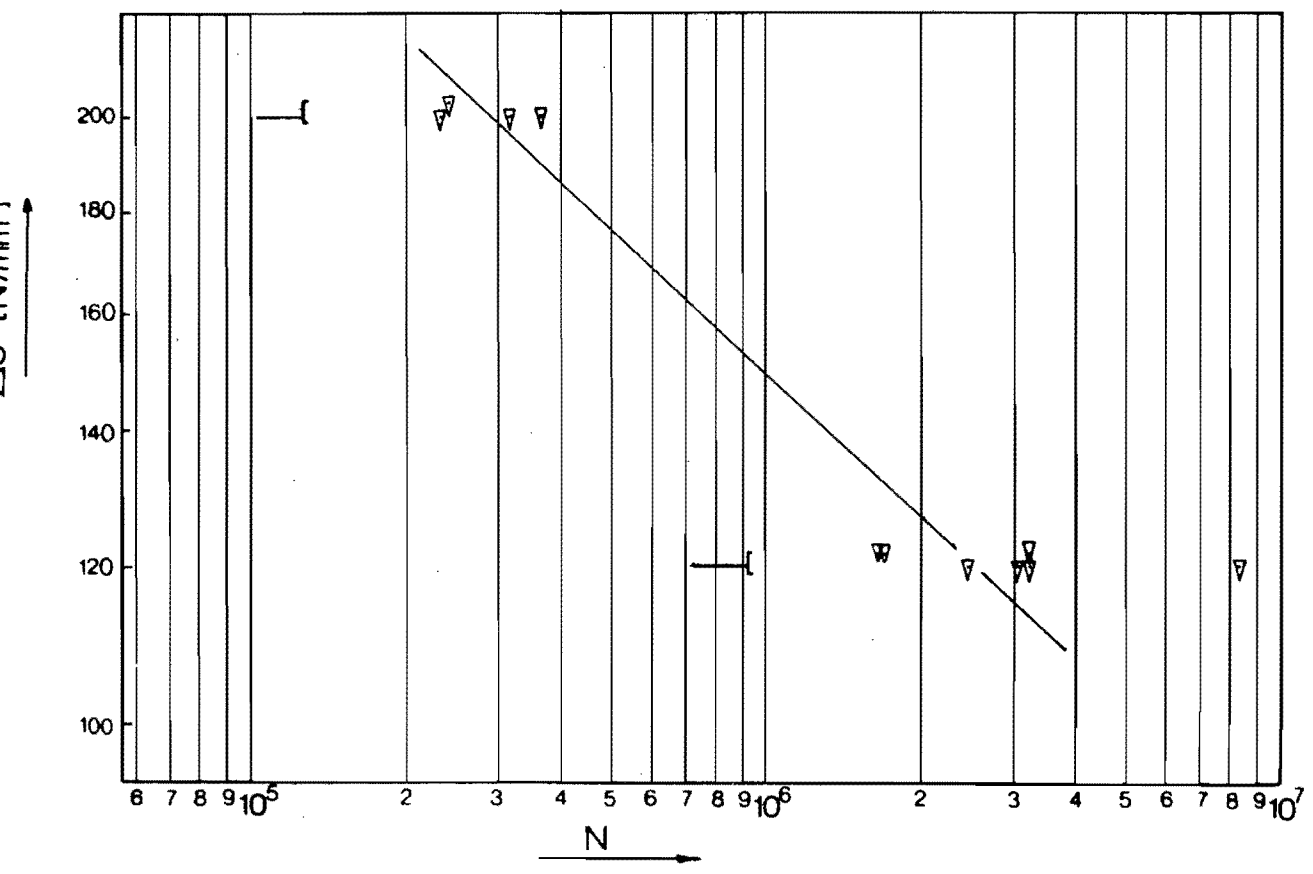

fig. 11 Endurances Series A16

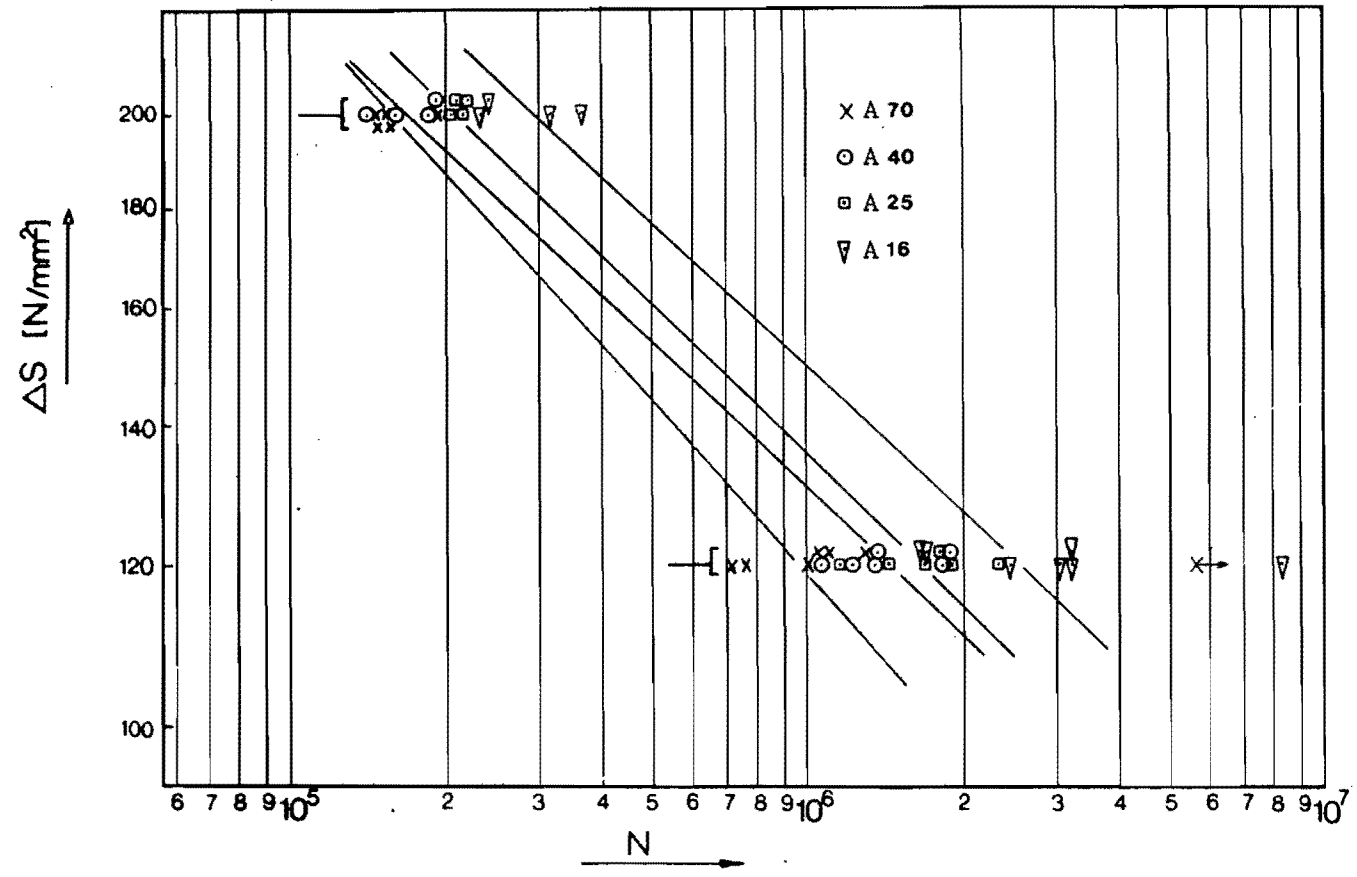

fig. 12 Endurances Series A70, A40, A25 and A16

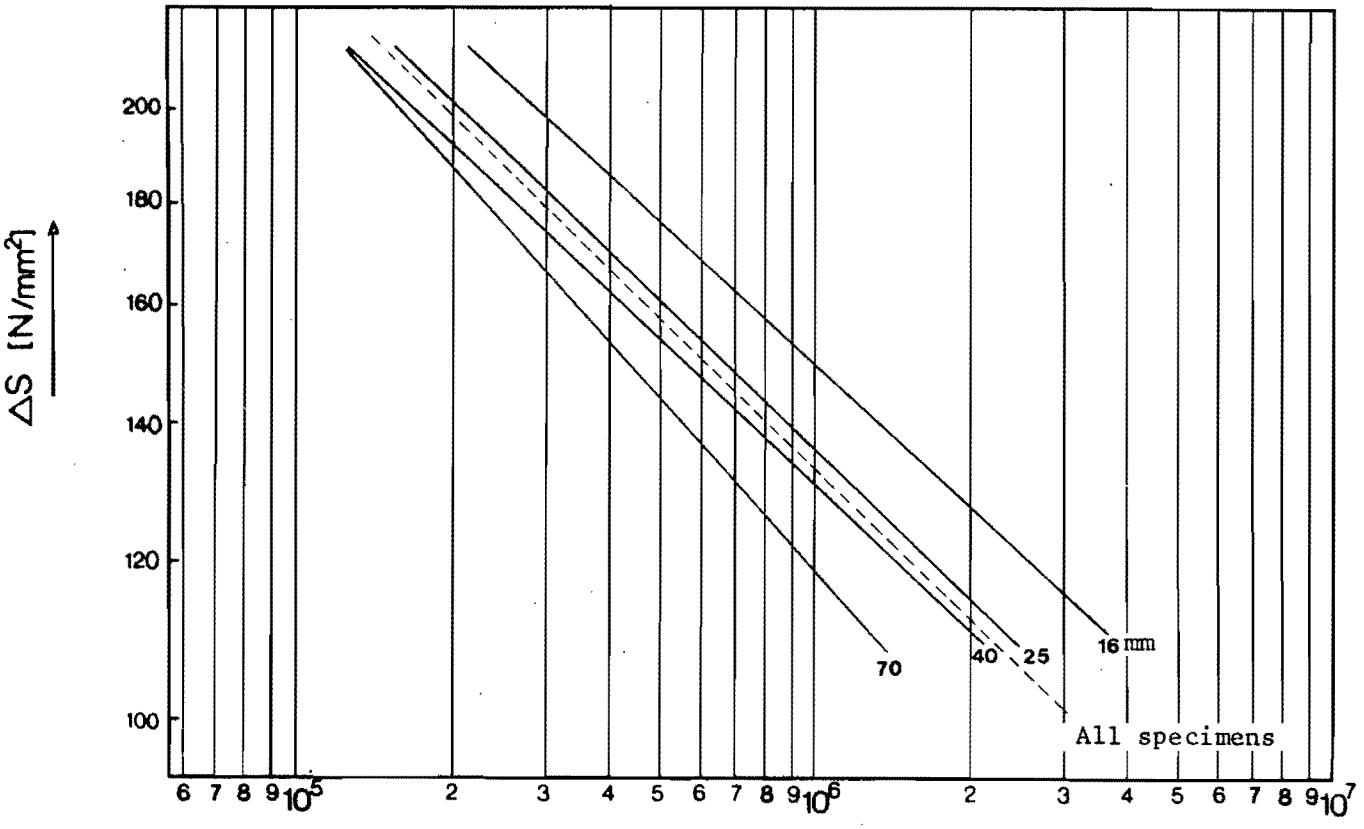

fig. 13 Regression lines

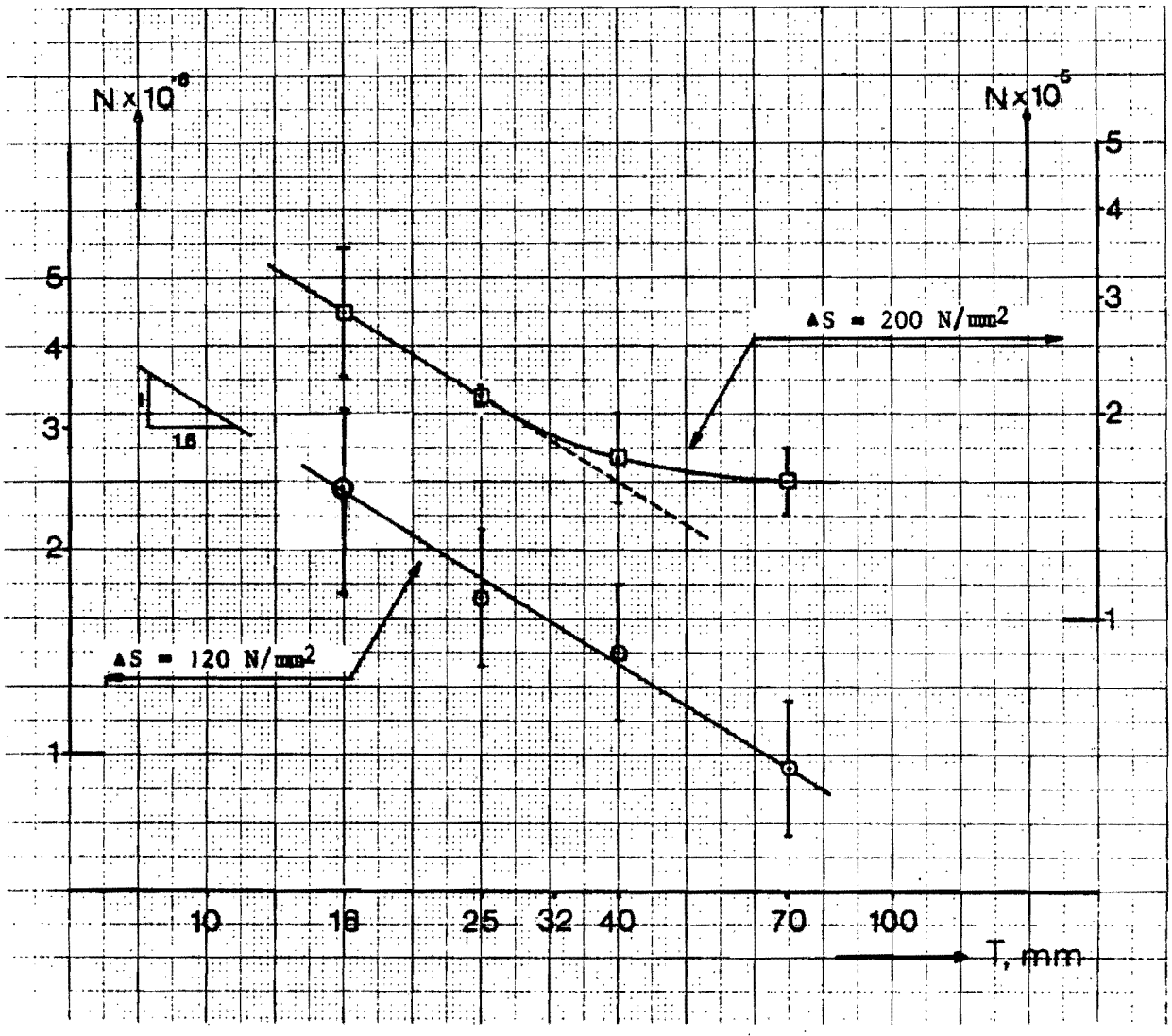

fig. 14 The effect of the thickness T on the endurance (see table 4)

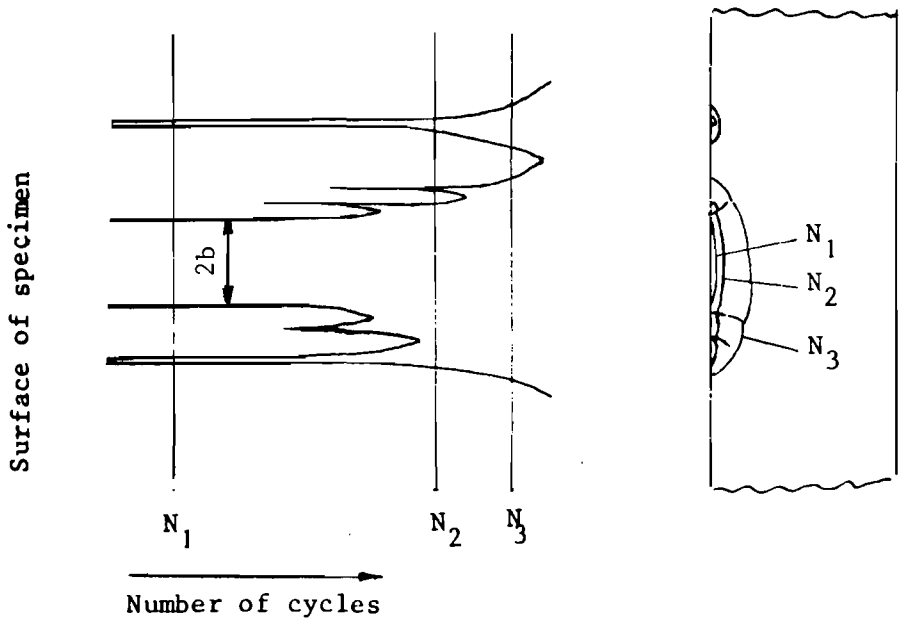

Fig. 15 A model for growth and coalescence of small cracks.

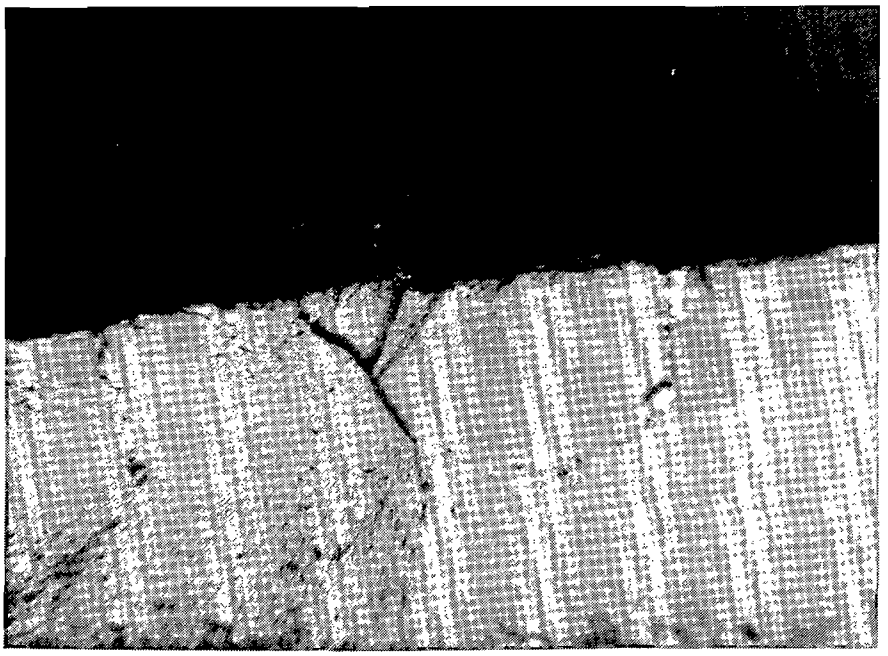

Fig, 16 Example of small secundary cracks and of step formation. (from unpublished work done in connection with[6]) V = 10x.

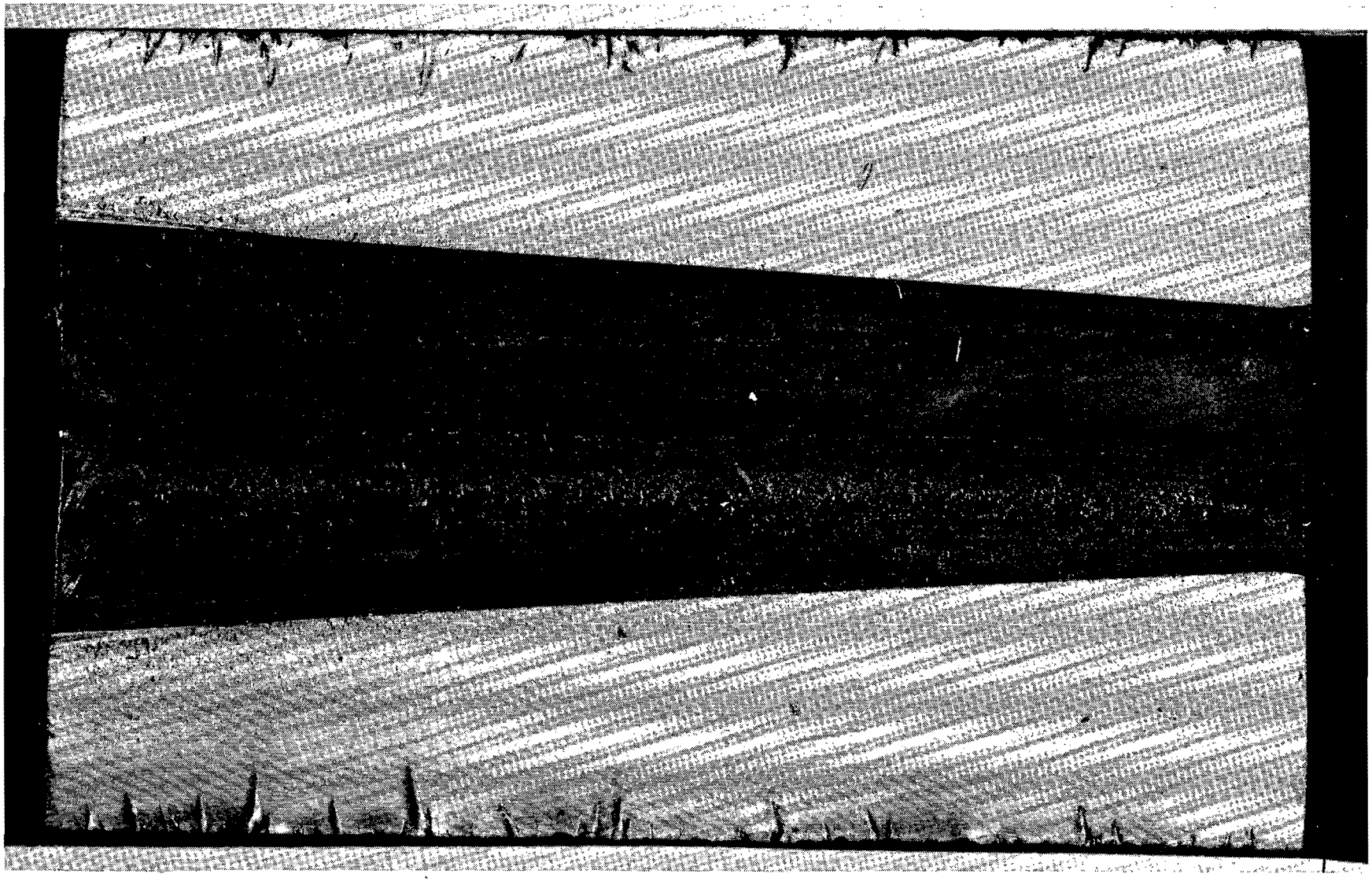

Fig. 17a. Fracture surface 70 mm specimen (scale 1:1).

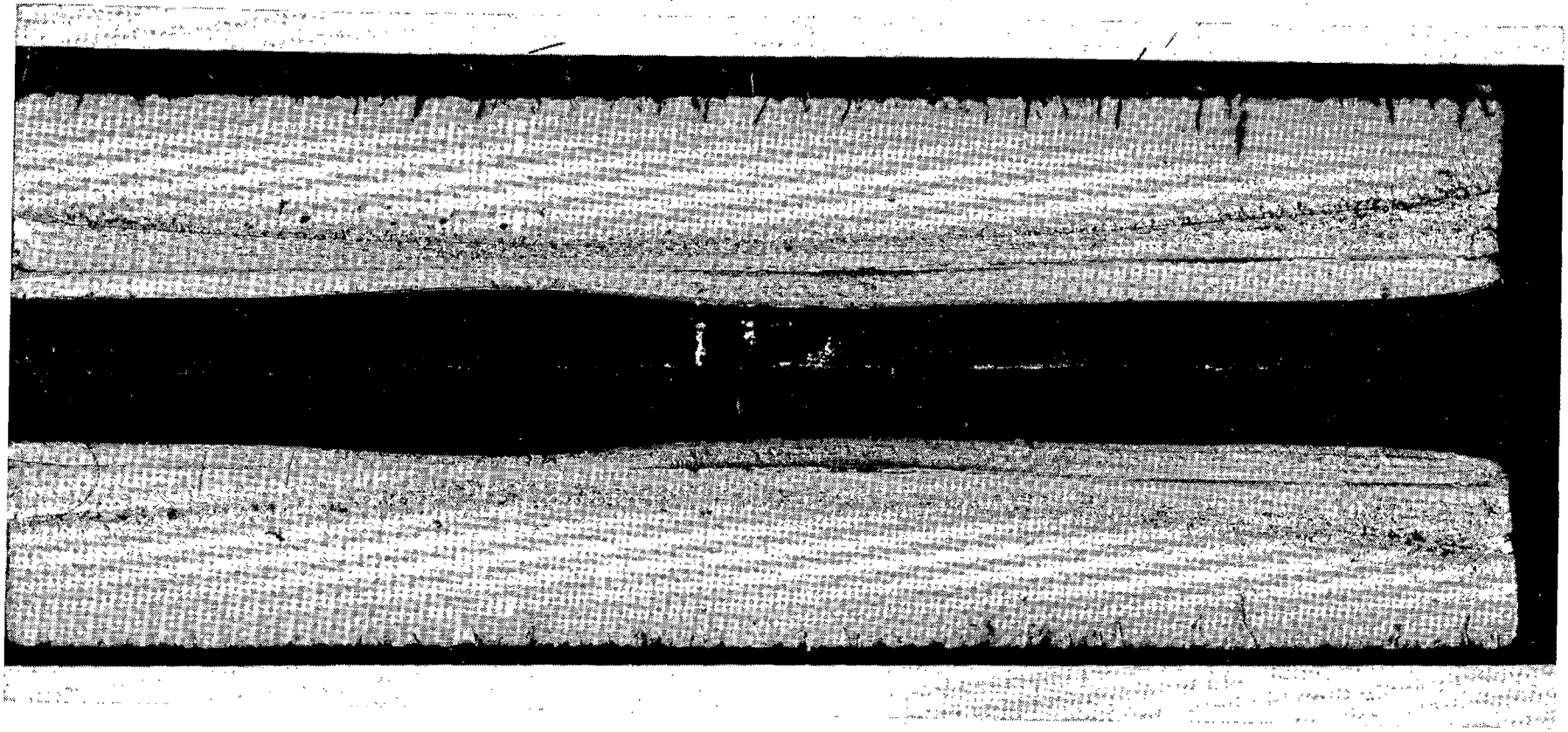

Fig. 17b. Fracture surface 40 mm specimen (scale 1:1).

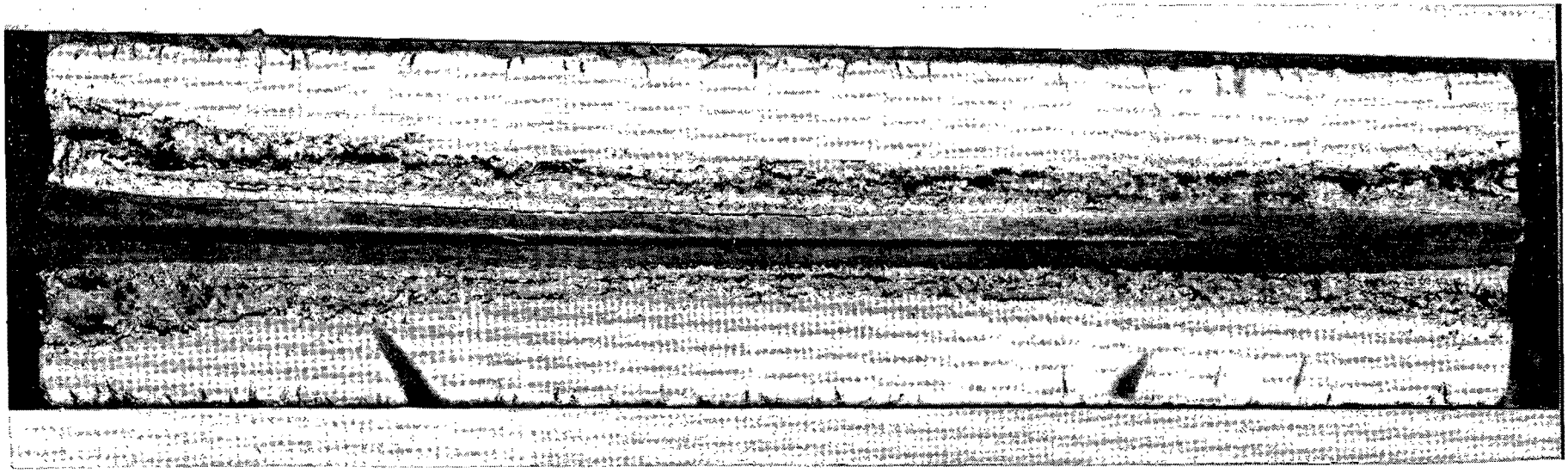

Fig. 17c. Fracture surface 25 mm specimen (scale 1:1).

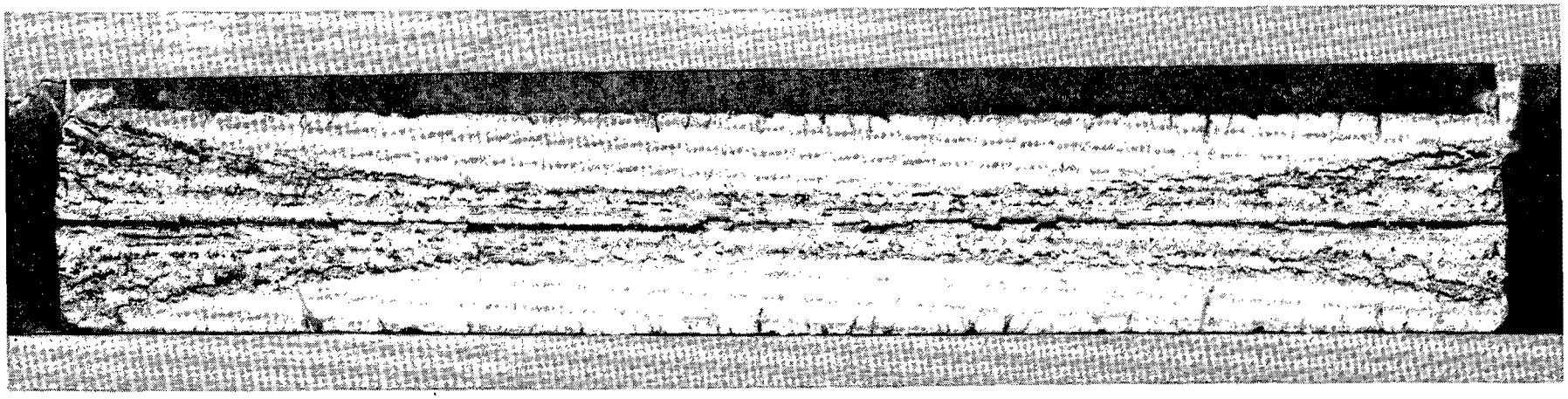

Fig. 17d. Fracture surface 16 mm specimen (scale 1:1).

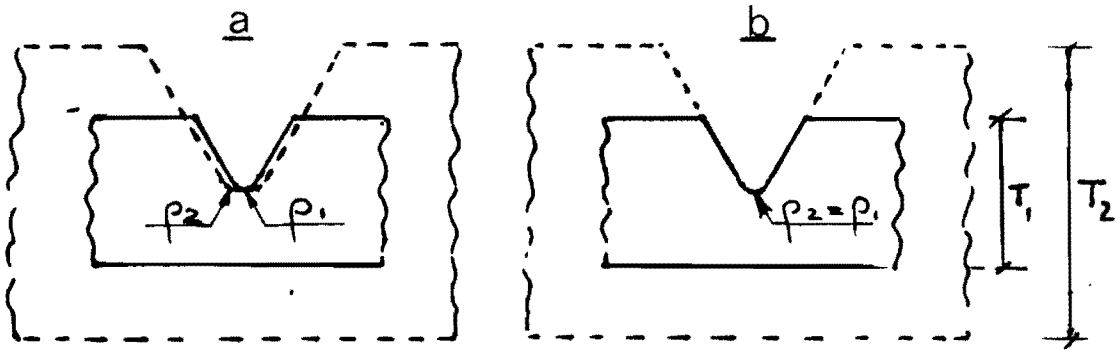

Fig. 18 Effect of (in)complete scaling up.

a. $T_{2/T_1} = \rho_{2/\rho_1} \rightarrow (K_t)_1 = (K_t)_2$

b. $T_{2/T_1} > 1$, $\rho_{2/\rho_1} = 1 \rightarrow (K_t)_1 < (K_t)_2$

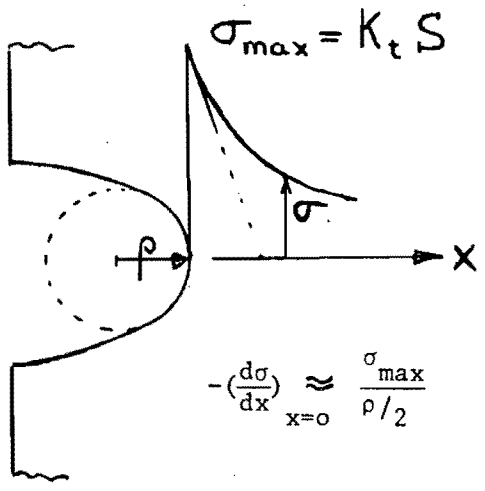

Fig. 19 Stress gradient near the notch root.

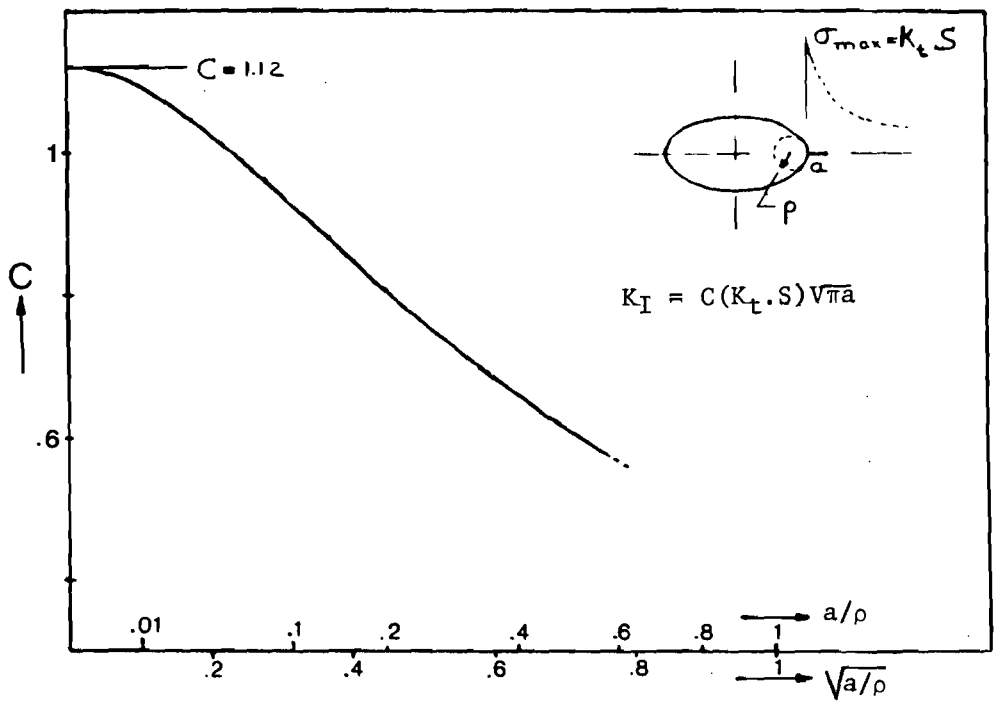

Fig. 20 : S.I.F. values according to [8] for small cracks emanating from elliptical holes of widely different aspect ratios (infinite plate loaded in tension).

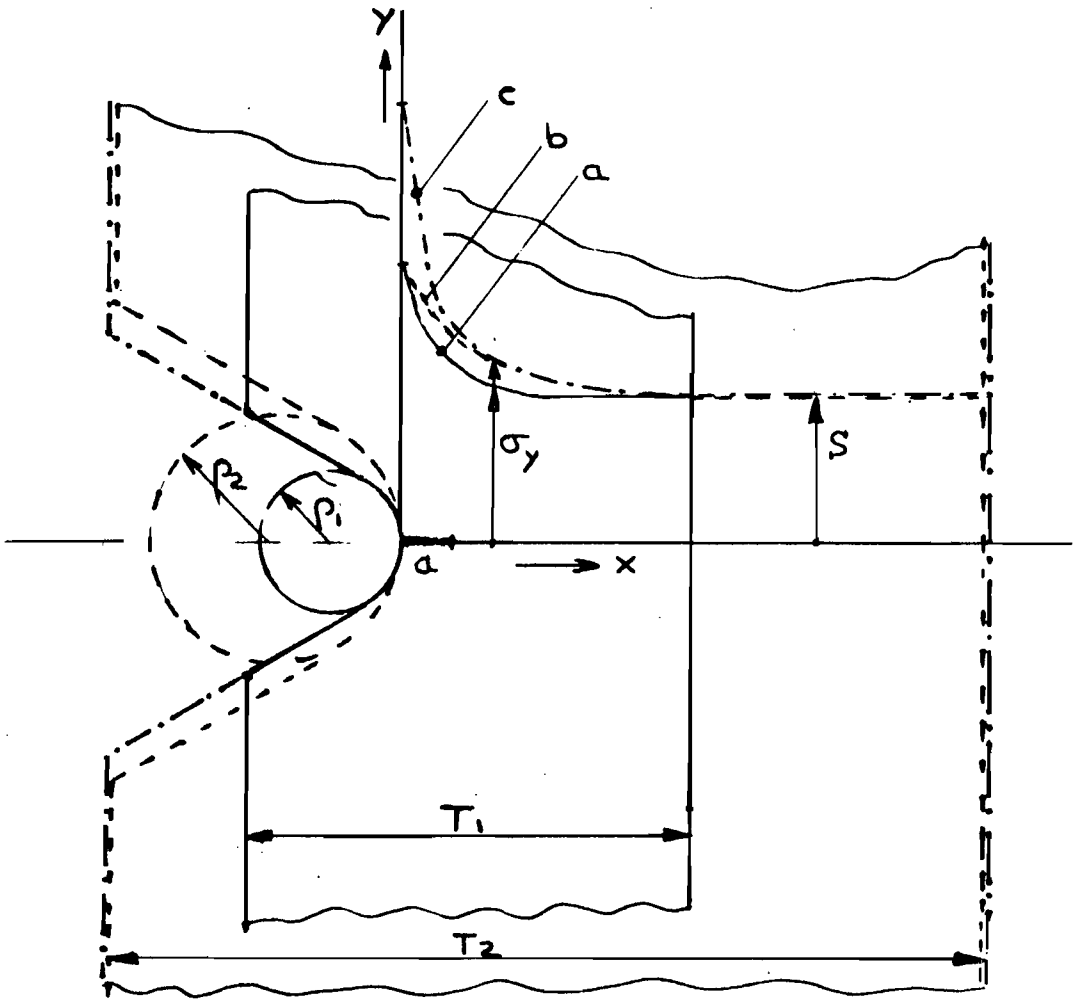

Fig. 21 σ_y as a function of x for incomplete scaling up at constant S.

a. —— T_1, ρ_1 (basic configuration): $(\sigma_{max})_1 = (K_t).S$

b. – – – $T_{2/T_1} = \rho_{2/\rho_1}$: $(\sigma_{max})_2 = (\sigma_{max})_1$

c. —·— $T_1/T_2 < 1$, $\rho_1 = \rho_2$ $(\sigma_{max})_2 > (\sigma_{max})_1$

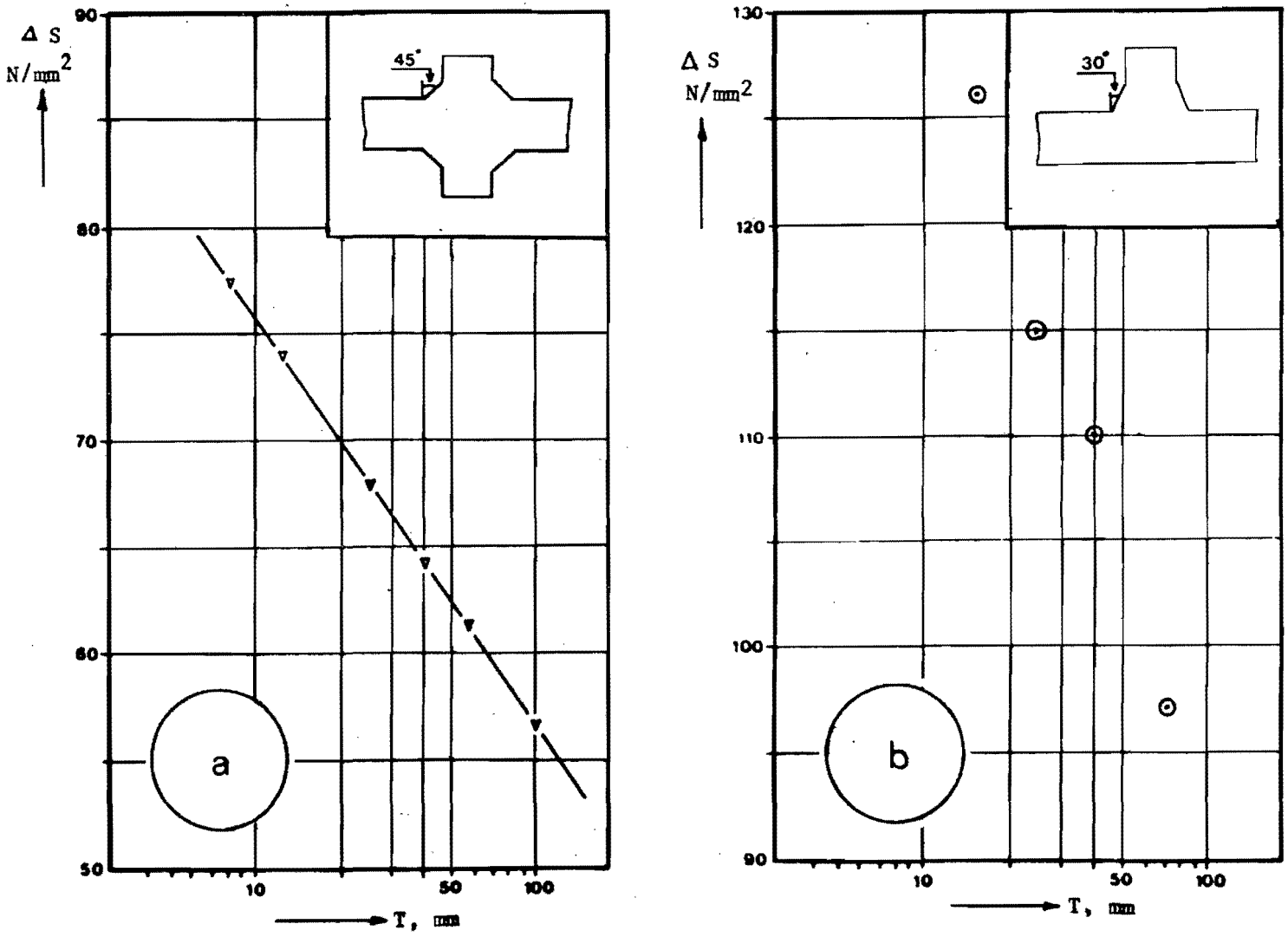

Fig. 22 Comparison of theoratical and experimental results at N= 2.10^6

a theoretical results from [10]

b experimental results from this investigation

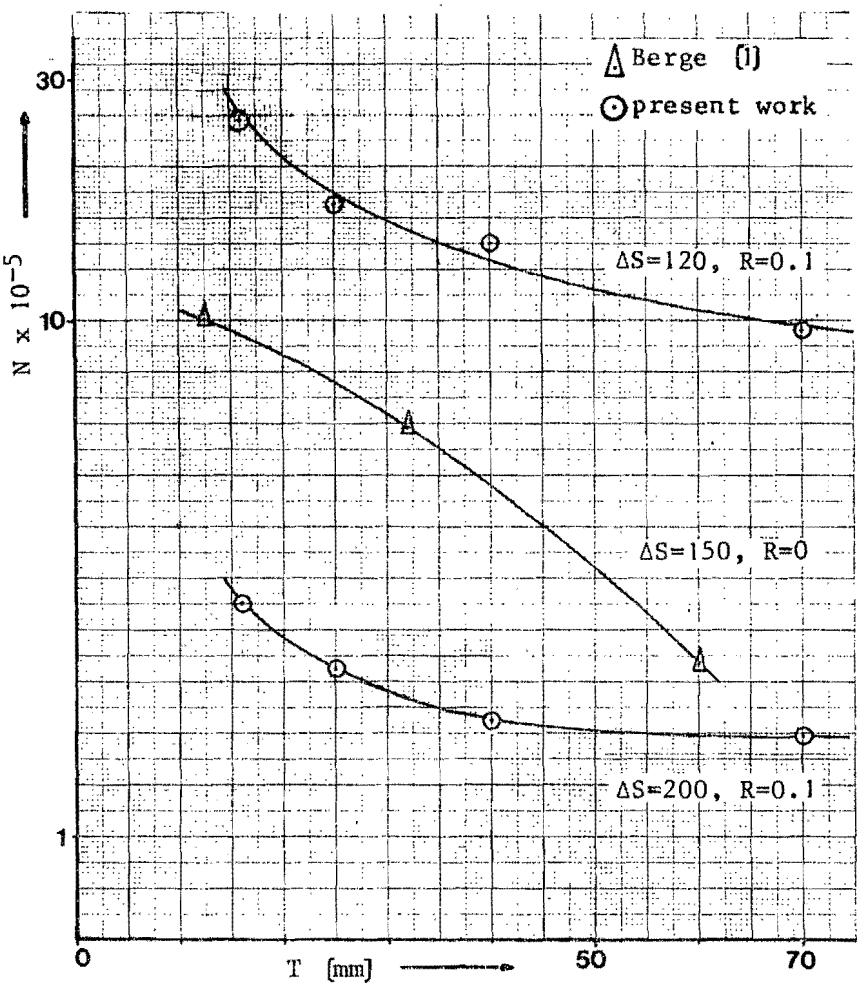

Fig.23a Scale effect reported in [1] in comparison with the results from tabel 4.
(note the linear scale for T)

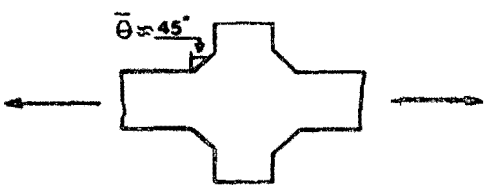

T (mm)	θ(deg)	ρ(mm)
12.5	39	2.2
32	30	2.7
60	54	1.8

Fig. 23b Specimens used in [1].